

**UNIVERSITY OF TURKISH AERONAUTICAL ASSOCIATION INSTITUTE  
OF SCIENCE AND TECHNOLOGY**

**DEVELOPMENT AND NUMERICAL TEST OF A GENERIC FLIGHT  
DYNAMICS MODEL OF A HELICOPTER**



**MASTER THESIS**

**Osman AYCI**

**Institute of Science and Technology**

**Mechanical and Aeronautical Engineering**

**SEPTEMBER 2016**

**UNIVERSITY OF TURKISH AERONAUTICAL ASSOCIATION INSTITUTE  
OF SCIENCE AND TECHNOLOGY**

**DEVELOPMENT AND NUMERICAL TEST OF A GENERIC FLIGHT  
DYNAMICS MODEL OF A HELICOPTER**



**MASTER THESIS**

**Osman AYCI**

**1303737011**

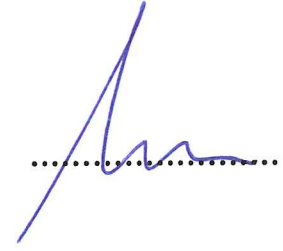
**Institute of Science and Technology**

**Mechanical and Aeronautical Engineering**

**Thesis Supervisor: Assoc. Prof. Dr. Mustafa KAYA**

Türk Hava Kurumu Üniversitesi Fen Bilimleri Enstitüsü'nün 1303737011 numaralı Yüksek Lisans öğrencisi, Osman AYCI ilgili yönetmeliklerin belirlediği gerekli tüm şartları yerine getirdikten sonra hazırladığı “DEVELOPMENT AND NUMERICAL TEST OF A GENERIC FLIGHT DYNAMICS MODEL OF A HELICOPTER” başlıklı tezini, aşağıda imzaları olan jüri önünde başarı ile sunmuştur.

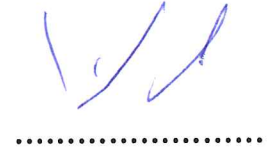
**Tez Danışmanı : Yrd. Doç. Dr. Mustafa KAYA**  
**Yıldırım Beyazıt Üniversitesi**



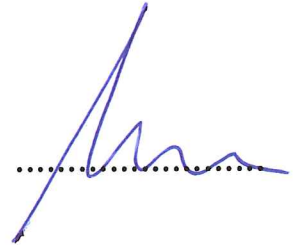
**Jüri Üyeleri : Doç.Dr. Murat DEMİRAL**  
**Türk Hava Kurumu Üniversitesi**



**: Yrd. Doç. Dr. Munir ELFARRA**  
**Yıldırım Beyazıt Üniversitesi**



**: Yrd. Doç. Dr. Mustafa KAYA**  
**Yıldırım Beyazıt Üniversitesi**



**Tez Savunma Tarihi : 09.09.2016**

**UNIVERSITY OF TURKISH AERONAUTICAL ASSOCIATION  
INSTITUTE OF SCIENCE AND TECHNOLOGY**

Submitted by Osman AYCI in partial fulfillment of the requirements for the degree of Master of Science in Mechanical and Aeronautical Engineering “DEVELOPMENT AND NUMERICAL TEST OF A GENERIC FLIGHT DYNAMICS MODEL OF A HELICOPTER” I hereby declare that all information in this document has been obtained and presented in accordance with academic rules and ethical conduct. I also declare that, as required by these rules and conduct, I have fully cited and referenced all material and results that are not original to this work.

02.09.2016  
Osman AYCI



## ACKNOWLEDGEMENTS

First, I would like to express my sincere gratitude to Assoc. Prof. Mustafa KAYA for his encouragement and supervision throughout my studies.

I want to emphasize my special thanks to Anıl Demirel, Murat Millidere and Volkan oşgun for their useful discussions about modeling. I also thank to them for their help about autopilot support and testing infrastructure to compare flight test data and simulation data.

I wish to state my thanks to Serhat Turhan, Aycan Okan, Harun Tayfun Söylemez and Ertuğrul Kartal Tabak for their support.

I would like to thank to Mehmet Yıldız, Hakan Sargın and Ebru Bulut for their support, encouragement and friendship.

I would also like to thank to my company HAVELSAN for supporting and encouraging me to write this dissertation.

Finally, I would like to express my deepest thanks to my parents for their endless support throughout my life.

September 2016

Osman AYCI

## TABLE OF CONTENT

ACKNOWLEDGEMENTS .....	iv
TABLE OF CONTENT .....	v
LIST OF FIGURES .....	vi
ABSTRACT .....	viii
ÖZET .....	x
<b>CHAPTER ONE</b> .....	1
<b>1. INTRODUCTION</b> .....	1
1.1 Simulation of Flight .....	1
1.2 Flight Test Data .....	3
1.3 Literature Survey .....	4
<b>CHAPTER TWO</b> .....	6
<b>2. GENERIC HELICOPTER MODEL</b> .....	6
2.1 Main Rotor Modeling .....	8
2.2 Main Rotor Model Theory .....	9
2.3 Tail Rotor Model Theory .....	21
2.4 Fuselage Model Theory .....	24
2.5 Horizontal Tail Model Theory .....	26
2.6 Vertical Tail Model Theory .....	27
<b>CHAPTER THREE</b> .....	30
<b>3. RESULTS</b> .....	30
3.1 First Test; 1 Inch Right Cyclic Step Input .....	31
3.2 Second Test; 1 Inch Aft Cyclic Pulse Input .....	35
3.3 Third Test; 0.5 Inch Collective Up Step Input .....	39
3.4 Fourth Test; 1 Inch Left Pedal Pulse Input .....	42
<b>CHAPTER FOUR</b> .....	47
<b>4. CONCLUSION</b> .....	47
<b>REFERENCES</b> .....	48
<b>APPENDIX</b> .....	50
Appendix-A: Symbol Definitions of Equations .....	51
<b>RESUME</b> .....	61

## LIST OF FIGURES

<b>Figure 2.1</b>	: Generic helicopter model block diagram representation.....	7
<b>Figure 2.2</b>	: Main rotor blade equal annuli area segment distribution .....	9
<b>Figure 2.3</b>	: Velocity and force components of blade segment.....	11
<b>Figure 2.4</b>	: Body to shaft axes transformation.....	11
<b>Figure 2.5</b>	: Shaft axes to blade span axes transformations .....	12
<b>Figure 3.1</b>	: Collective input. ....	32
<b>Figure 3.2</b>	: Roll input.....	32
<b>Figure 3.3</b>	: Pitch input. ....	32
<b>Figure 3.4</b>	: Yaw input. ....	32
<b>Figure 3.5</b>	: Roll attitude.....	33
<b>Figure 3.6</b>	: Pitch attitude.....	33
<b>Figure 3.7</b>	: Yaw attitude. ....	33
<b>Figure 3.8</b>	: Roll rate. ....	34
<b>Figure 3.9</b>	: Pitch rate.....	34
<b>Figure 3.10</b>	: Yaw rate. ....	34
<b>Figure 3.11</b>	: Vertical speed. ....	35
<b>Figure 3.12</b>	: Indicated air speed.....	35
<b>Figure 3.13</b>	: Collective input. ....	35
<b>Figure 3.14</b>	: Roll input.....	36
<b>Figure 3.15</b>	: Pitch input. ....	36
<b>Figure 3.16</b>	: Yaw input. ....	36
<b>Figure 3.17</b>	: Roll attitude.....	36
<b>Figure 3.18</b>	: Pitch attitude.....	37
<b>Figure 3.19</b>	: Yaw attitude. ....	37
<b>Figure 3.20</b>	: Roll rate. ....	37
<b>Figure 3.21</b>	: Pitch rate.....	38
<b>Figure 3.22</b>	: Yaw rate. ....	38
<b>Figure 3.23</b>	: Vertical speed.....	38
<b>Figure 3.24</b>	: Indicated air speed.....	38
<b>Figure 3.25</b>	: Collective input. ....	39
<b>Figure 3.26</b>	: Roll input.....	39
<b>Figure 3.27</b>	: Pitch input. ....	39
<b>Figure 3.28</b>	: Yaw input. ....	39
<b>Figure 3.29</b>	: Roll attitude.....	40
<b>Figure 3.30</b>	: Pitch attitude.....	40
<b>Figure 3.31</b>	: Yaw attitude. ....	40
<b>Figure 3.32</b>	: Roll rate. ....	41
<b>Figure 3.33</b>	: Pitch rate.....	41
<b>Figure 3.34</b>	: Yaw rate. ....	41
<b>Figure 3.35</b>	: Vertical speed.....	42
<b>Figure 3.36</b>	: Indicated air speed.....	42

<b>Figure 3.37</b> : Collective input. ....	42
<b>Figure 3.38</b> : Roll input. ....	43
<b>Figure 3.39</b> : Pitch input. ....	43
<b>Figure 3.40</b> : Yaw input. ....	43
<b>Figure 3.41</b> : Roll attitude. ....	43
<b>Figure 3.42</b> : Pitch attitude. ....	44
<b>Figure 3.43</b> : Yaw attitude. ....	44
<b>Figure 3.44</b> : Roll rate. ....	45
<b>Figure 3.45</b> : Pitch rate. ....	45
<b>Figure 3.46</b> : Yaw rate. ....	45
<b>Figure 3.47</b> : Vertical speed. ....	46
<b>Figure 3.48</b> : Indicated air speed. ....	46





## **ABSTRACT**

### **DEVELOPMENT AND NUMERICAL TEST OF A GENERIC FLIGHT DYNAMICS MODEL OF A HELICOPTER**

AYCI, Osman

Master, M.S. in Mechanical and Aeronautical Engineering

Thesis Supervisor: Assoc. Prof. Mustafa KAYA

September 2016, 60 page

The flight training simulators are widely used in pilot training programs. For manned helicopters, flight simulators are very common to use, not only to reduce time and cost of training activities, but also to prevent possible loss of pilot or aircraft in case of any circumstances. Flight simulators decrease pilot errors in different weather conditions and possible malfunctions of critical systems. In order to increase the quality of the training, higher fidelity helicopter models are required in flight simulators. The higher the fidelity, the better the training as long as real-time constraints are satisfied. Generic helicopter model is developed to meet this critical and important demand. This model is a high fidelity generic helicopter model simulating all major components of a helicopter. The most important components include rotors, engine, automatic flight control system (AFCS). This thesis study presents the flight dynamic simulation model of this generic helicopter model. An adaptive and flexible structure is designed to implement all design parameters reflecting the flight characteristics of a helicopter. By using this structure, the model is adapted to the target helicopter. The main structure is built in MATLAB & Simulink environment. Certain models are developed in C++ and used as a library in Simulink. The capability is demonstrated by validating the model against Blackhawk (UH-60) flight test data. The flight tests are selected from Qualification Test Guide

(QTG) defined by certification standards for helicopter flight simulation training devices.

**Keywords:** Flight dynamics; Mathematical Modeling; Simulation; Helicopter



## ÖZET

### JENERİK HELİKOPTER UÇUŞ DİNAMİĞİ MODELİ GELİŞTİRİLMESİ VE SAYISAL TESTİ

AYCI, Osman

Yüksek Lisans Tezi, Makina ve Uçak Mühendisliği Anabilim Dalı

Tez Danışmanı: Yrd. Doç. Dr. Mustafa KAYA

Eylül 2016, 60 sayfa

Uçuş Eğitim Simülatörleri pilot eğitim programlarında yaygın olarak kullanılmaktadır. İnsanlı helikopterler için, uçuş simülatörleri sadece zaman ve eğitim faaliyetlerinin maliyetini azaltmak için değil, aynı zamanda her koşul ve durumda pilotun veya uçağın olası kaybını önlemek için de kullanılmaktadır. Uçuş simülatörleri, farklı hava koşulları ve kritik sistemlerin olası arızaları sırasında pilot hatalarını azaltır. Uçuş simülatörlerinde eğitim kalitesini artırmak için, yüksek sadakat seviyeli helikopter modeli gereklidir. Gerçek zamanlı çalışma kısıtlarını yerine getirdiği sürece, daha yüksek sadakat seviyesi, daha yüksek eğitim kalitesi anlamına gelir. Jenerik Helikopter Model bu kritik ve önemli talebi karşılamak için geliştirilmiştir. Bu model bir helikopterin tüm önemli bileşenlerini simüle eden yüksek sadakat seviyeli jenerik helikopter modelidir. En önemli bileşenler, rotor, motor, otomatik uçuş kontrol sistemini (AFCS) içerir. Bu tez çalışması jenerik helicopter modelinin uçuş dinamik simülasyon modelini içerir. Bir helikopterin uçuş karakteristiğini yansıtan tüm tasarım parametrelerini kullanmak için uyarlanabilir ve esnek bir yapı tasarlanmıştır. Bu yapı kullanılarak, model hedef helikoptere uyarlanabilmektedir. Ana yapı MATLAB & Simulink ortamında oluşturulmuştur. Belli modeller C ++ ortamında geliştirilmiş ve Simulink için bir kütüphane olarak kullanılmaktadır. Jenerik helikopter modelinin yeteneği Blackhawk (UH 60) uçuş

test verileri ile doğrulanarak kanıtlanmıştır. Uçuş testleri helikopter uçuş simülasyon eğitimi cihazları sertifikasyon standartlarına göre tanımlanan Qualification Test Guide (QTG) kapsamındaki testlerden seçilmiştir.

**Anahtar Kelimeler:** Uçuş Dinamiği; Matematik Modelleme; Simülasyon; Helikopter



## **CHAPTER ONE**

### **INTRODUCTION**

During design and development of an aircraft, it needs to be tested with different design parameters to find out the best configuration of design and its performance limits need to be validated. To reduce time and cost during the design testing phase, simulations are preferred. Flight simulations is not only used for design process but also at pilot training programs. For manned flight vehicles flight simulators are very common to use before real flight, not only to reduce time and costs during the testing phase, but also to prevent possible loss of pilot and aircraft in case of a failure. Therefore, The flight training simulators are widely used at pilot training programs. A brief description of desired capability and capacity of real flight simulators in general will follow.

#### **1.1 Simulation of Flight**

In commercial and military applications, rotorcraft and its capabilities of vertical take-off and landing, hover, vertical and forward flight are playing an important role. Hover and low speed performance and agility are combined with good flight characteristics even in fast forward flight. In all flight conditions, the rotor of a helicopter produces the predominant aerodynamic forces. It is source of forces and moments on the aircraft that control position, attitude and velocity. The development of detailed mathematical models of rotors and helicopters is complicated because of an increase of complexity with respect to rotor and blade dynamics and the still not sufficiently explained aerodynamic effects of rotor aerodynamic or rotor-body interference.

The capability of mathematical models for simulation is therefore limited to some degree of accuracy and its fidelity depends on the objective of the simulation.

Helicopter's unique capabilities determine the effort and expense needed for modeling and simulation, and also the simulation objective effects the level of fidelity of the mathematical model which is directly related to the effort and expense required for a given task.

Accuracy of simulation increased with the help of high performance computers, but the complexity of simulation still rules the capability of operating in real-time. The development and validation of high-fidelity real-time simulator is strongly dependent on available time and money. Once developed and validated, the simulator can be very efficiently used to support flight tests to evaluate handling qualities during the development and design phase of new or modified helicopter configurations or helicopter components. Applications of unconventional configurations like tilt wings and tilt rotors, simulating emergency situations, validating and testing new control systems or simple pilot training show importance of use of such a high-fidelity real-time simulator. Nevertheless, complex system which includes highly accurate model of one component does not necessarily mean that the simulation of the whole system behaves like the real physical system. This situation is valid especially for a helicopter, because of components like rotors, wings, fuselage, horizontal or vertical tail interact with each other. This interactions effect the system response to external and internal disturbances.

In helicopter control applications, it is necessary to find a representative mathematical model that shows the same dynamic characteristics as the real aircraft because the main objective is to control the dynamic behavior of the helicopter. Since dynamics are governed mainly by the main rotor, a detailed model of the main rotor is desired; on the other hand, a too detailed model increases the complexity of the simulation and limits the capability of real-time simulation. Furthermore, most of the existing simulations make a very detailed knowledge of the simulated system necessary. This knowledge includes exact physical data of the aircraft geometry, blade and wing airfoils and aerodynamic data gained in wind tunnel tests. This data is handled by companies with care for competitive reasons and is therefore generally not available. Therefore, in literature, it is hard to find geometric and aerodynamic data for high fidelity helicopter models. Since detailed data is available in literature for Blackhawk (UH-60), its geometric and aerodynamic data is used in this work.

Even if satisfying results can be achieved with a high-fidelity real-time simulator, the results will not be sufficient unless they are confirmed in real flight. Flight test data is available in literature. For this reason, to confirm the model, Blackhawk (UH-60) flight test data is used.

In summary, the main attribute of a simulator as an effective tool for controller design is the ability to produce desired results for a specific application and to operate over the full flight envelope (forward, rearward and sideward flight, hover, transition from hover to forward flight, vertical climb) with representative handling qualities. Through a man-in-the-loop simulation it also becomes a very powerful tool to identify critical man-machine or controller-machine interface issues and allow pilot training within a reasonable amount of time, costs and risk until confidence in flying with a new system or flight controller is gained.

## **1.2 Flight Test Data**

The test data used for comparison were obtained in a series of tests conducted by USAAEFA for use in validation of the Rotorcraft Systems Integration Simulator. No stability augmentation was used during transient-response test runs. Analog and digital stability augmentation systems, the flightpath stabilization system, and the stabilator control system were disabled and the pitch bias actuator was centered and locked.

The transient responses consisted of individual-axis steps, pulses, or doublets of one inch or less. The test procedure normally consisted of stabilizing in trim with one of the two redundant stability augmentation systems on; this was disabled one second before the control input. Unsatisfactory stability characteristics of the unaugmented aircraft, especially in pitch, required the pilot to initiate recovery within a few seconds of the input. Because of pilot difficulty in maintaining trim of the unaugmented aircraft, in many cases flight-test data had drifted from trim at the time of the control input, causing differences between test and simulation responses.

The outline of this thesis is as follows: Next section includes literature survey. After literature survey, modeling details are described and finally simulation and flight test data comparison results are presented.

### 1.3 Literature Survey

In 1941, the National Advisory Committee of Aeronautics (NACA) published a report [1], which provides a simplified theoretical main rotor model in forward flight. This model includes expressions for the flapping, torque, thrust and profile drag of hinged, rectangular, linearly twisted blades as functions of inflow velocity and blade pitch angle. In 1979, a paper published by Robert T. N. Chen that has focused on main rotor dynamics [2]. Real time pilot-in-the-loop investigation of helicopter flying qualities was the purpose of this study. Robert T. N. Chen developed a detailed model of the flapping motion of the main rotor in 1980 [3]. In this study [3], the effect of primary rotor parameters such as pitch-flap coupling, blade Lock number, flapping hinge offset and flapping hinge restraint on the flapping dynamics were investigated. To analyze the effect of these design features on flapping dynamics with regard to the influence on agility, stability, and operational safety of helicopters was the aim of the study. A full mathematical model of a classical single rotor helicopter was developed for piloted simulation in 1982 [4]. Most of the components of the helicopter such as main rotor with flapping and uniform inflow, tail rotor, fuselage, horizontal and vertical tail are included in this model.

Another study was performed within a NASA Contract about modeling a UH-60A Helicopter by Sikorsky Helicopter. In 1981, in order to perform an engineering simulation for performance and handling qualities evaluations, J.J. Howlett of Sikorsky issued a NASA Contractor Report regarding a UH-60A Black Hawk engineering simulation program, which was a project for the US Army [5]. This work is taken as the base for the helicopter model that has been developed in this thesis study. 3 years later, a NASA Technical Memorandum was published about a mathematical model of UH-60 Black Hawk helicopter by K. B. Hilbert of NASA [6]. This memorandum was performed as a revision of the previous work carried out by Howlett. Certain components of the UH-60 model such as fuselage, tail rotor and horizontal stabilizer were updated in this memorandum. One year later, in 1985, another contractor report for NASA was carried out by Thaddeus T. Kaplita of Sikorsky Helicopter which is regarding the validation of the UH-60 model which is explained in the work of Howlett [7]. In this work [7], model was validated by flight test data and according to the flight test data some modifications were done to the



existing model. In 1986, a technical report about a full mathematical model of a helicopter were published by Robert Hefley and Marc Mnich of NASA Ames Research Center [8]. This paper concentrated on the minimum required fidelity of a mathematical model of UH-60 helicopter for real time simulation applications. To develop a simple model that only included the primary properties of a helicopter that the pilot can perceive was the main purpose of this work.



## CHAPTER TWO

### GENERIC HELICOPTER MODEL

Generic helicopter model is developed to meet the critical and important demand on higher fidelity satisfying real-time constraints. The major design objective of this helicopter model is to develop a high fidelity generic helicopter model simulating all major components of a helicopter, including main rotor, autopilot and engine components. Main rotor model is based on the reputable GENHEL model [5].

The main framework is developed in MATLAB & Simulink environment. Model components are developed in C++ and used as a library in MATLAB & Simulink.

Specific advantages obtained from this work environment are listed as follows;

1. Clear identification of the mathematical model by the help of block diagrams
2. The data flow between model components can be observed during simulation running
3. Easy integration with visual software such as Flightgear
4. Pilot control inputs can be easily given into the model
5. Completed model software can be reused as software libraries in simulation environments

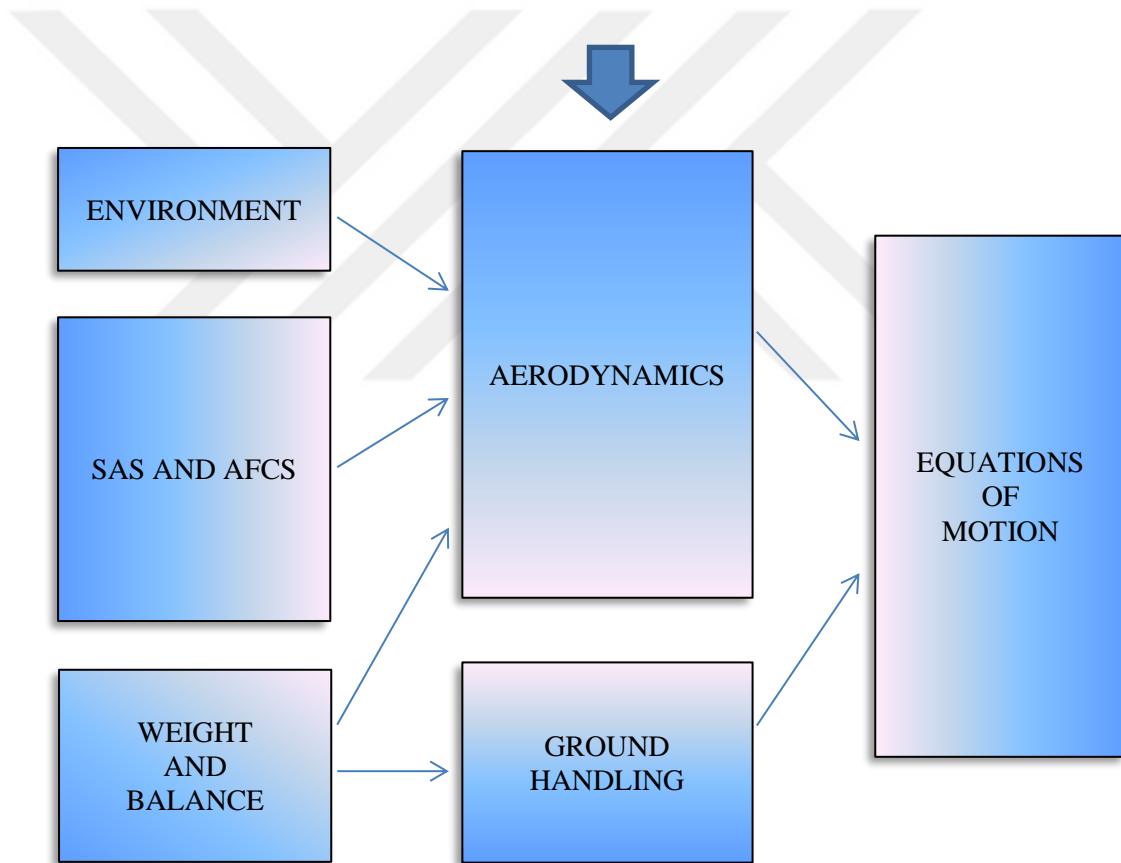
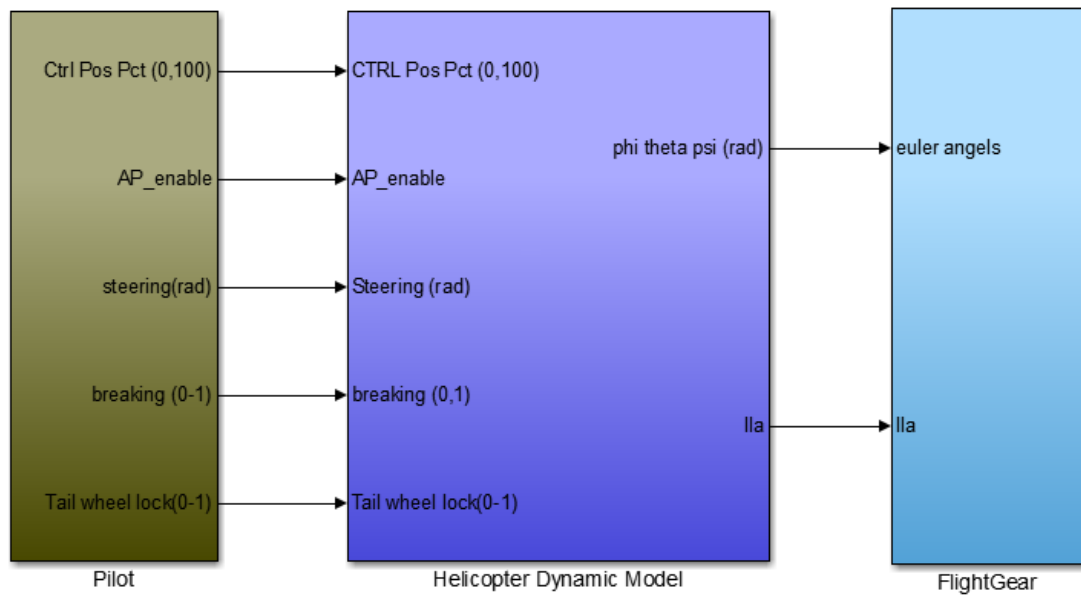


**Figure 2.1:** Generic helicopter model block diagram representation.

The main diagrams for helicopter dynamic model is presented in Figure 2.1. Environmental Model, Weight and Balance, Ground Handling, Flight Control System (FCS) and Automatic Flight Control System (AFCS), Aerodynamics and 6-DOF (Degree of Freedom) Equations of Motion are main blocks. Environment block

calculates temperature, air pressure and air density. Aerodynamics block include main and tail rotor, fuselage and horizontal and vertical tail sub-models. The general structure of aerodynamics block models are based on GEN-HEL model. FCS and AFCS blocks include flight control system, stability augmentation system (SAS) and autopilot modes such as altitude hold, air speed hold. Ground handling model includes landing gear and ground interaction computations. Weight and Balance block includes moment of inertia, total weight calculations and determination of center of gravity location. Translational and rotational accelerations, velocities and positions are calculated from total forces and moments affecting on the helicopter in different flight regimes by Equations of Motion block.

List of required models in a rotary wing simulation includes main and tail rotor, transmission/drive train, control systems, landing gear, fuselage, engines, horizontal and vertical tail and mutual interference effects and atmosphere [9].

## **2.1 Main Rotor Modeling**

Modeling of helicopter dynamics and especially rotor dynamics modeling is a complex work. Many approaches have been developed which is taking into account real-time performance parameters. Each approach attempts to reach varying physical degree of accuracy in the modeling. It should be noted that degree of accuracy has been primarily driven by the real-time processing requirements and computational limitations. Braman et.al classifies these approaches in four categories: Perturbation Models, Rotor Disc Models, Rotor Blade Map Models, and Blade Element Rotor Models [10].

One of the high quality approaches used for rotor modeling is Blade Element Rotor Model (BERM) [11]. BERM is the selected model for main rotor simulation. In this model, the forces on each blade element due to its motion through the air and hence the performance of the entire rotor are calculated. This model assumes that each blade element acts as a two-dimensional airfoil section producing aerodynamic forces which are then numerically integrated along the blade span. Virtual blades that are distributed through equal azimuth angle intervals over the rotor disk area are constructed to obtain more realistic solution results. The virtual blades are divided into small sections (segments) from root to the tip of the blade. The detailed description and formulation can be found on related books [11] [12] [13].

According to the theory of BERM, the blade can be interpreted as a set of infinitesimal airfoil elements, and their physical properties are integrated along the blade. Airfoil elements are actually a slice of the blades. The blades collide with air molecules generating lift and drag forces. The calculated forces on each blade component are aggregated by performing all required coordinate system transformations [14].

## 2.2 Main Rotor Model Theory

The main rotor model is based on a blade element analysis in which total rotor forces and moments are developed from a combination of aerodynamic, mass and inertia loads acting on each blade. The blade segment setup option defined as equal annuli area swept by the segment which allows the number of segments to be minimized and distributes the segments towards the higher dynamic pressure areas

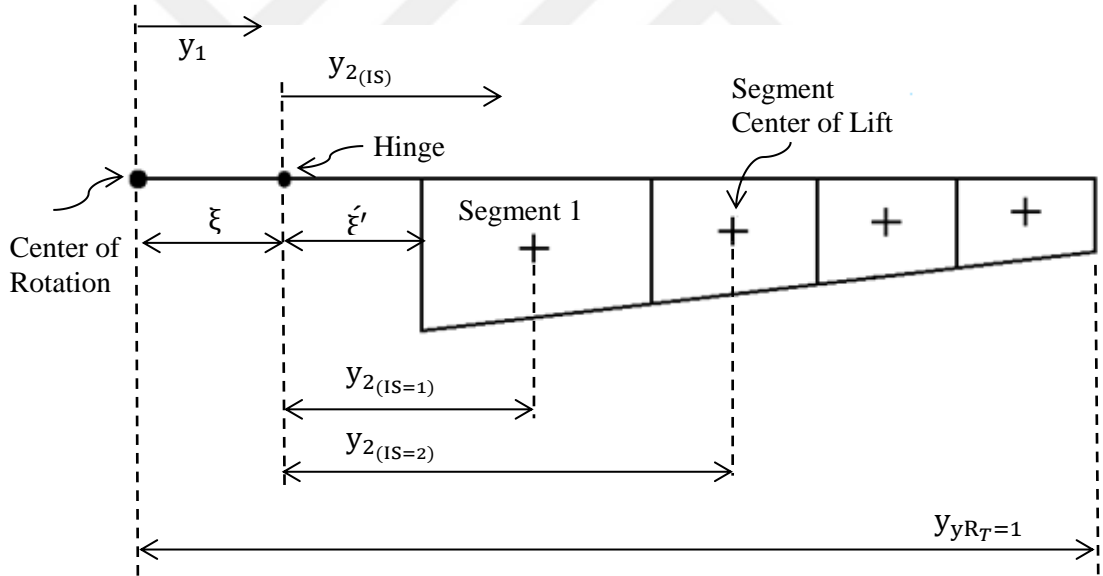


Figure 2.2: Main rotor blade equal annuli area segment distribution [5].

where “ $e$ ” is the hinge offset and “ $\acute{e}$ ” is the cut-out length and  $R_T$  is the rotor radius. Hinge offset and cut-out lengths are normalized by the rotor radius.

$$e = \frac{\xi}{R_T} \quad (\text{Eqn.2.1})$$

$$\acute{e} = \frac{\xi'}{R_T} \quad (\text{Eqn.2.2})$$

Actual blade length (Normalized by  $R_T$ )

$$1 - e - \acute{e} \quad (\text{Eqn.2.3})$$

First segment midpoint (which is defined as center of lift) “y” location is;

$$y_{21} = \left\{ \left[ \frac{1 - (e + \acute{e})^2}{2 * NSS} \right] + (e + \acute{e})^2 \right\}^{1/2} - e \quad (\text{Eqn.2.4})$$

where NSS is number of blade segments which depends on how many blade segments you want to split up its recommended that lots of blade segments through the blade tip gives more accurate solutions.

The other segments midpoints should be determined by,

$$y_{2IS} = \left\{ \left[ \frac{1 - (e + \acute{e})^2}{NSS} \right] + (e + y_{2IS-1})^2 \right\}^{1/2} - e \quad (\text{Eqn.2.5})$$

where IS means indicating segment. The segments “y” locations should be obtained by this equation above except first blade segment. After definitions of “y” locations, the segment widths will be,

$$\Delta y_{IS} = y_{\text{outbord}_{IS}} - y_{\text{inbord}_{IS}} \quad IS = 1, 2, \dots, NSS \quad (\text{Eqn.2.6})$$

where,

$$y_{\text{outbord}_{IS}} = \left\{ (y_{2IS} + e)^2 + \left[ \frac{1 - (e + \acute{e})^2}{2 * NSS} \right] \right\}^{1/2} \quad (\text{Eqn.2.7})$$

$$y_{\text{inbord}_{IS}} = \left\{ (y_{2IS} + e)^2 - \left[ \frac{1 - (e + \acute{e})^2}{2 * NSS} \right] \right\}^{1/2} \quad (\text{Eqn.2.8})$$

And Segments mean chord becomes,

$$C_{y_{IS}} = \left[ \left( \frac{C_T - C_R}{1 - e - \acute{e}} \right) \left( \frac{y_{\text{outbord}_{IS}} + y_{\text{inbord}_{IS}} - 2(e + \acute{e})}{2} \right) \right] + C_R \quad (\text{Eqn.2.9})$$

$C_T$  and  $C_R$  are tip chord and root chord of the blade respectively. Segment are finally can be calculated by,

$$S_{y_{IS}} = (R_T)(C_{y_{IS}})(y_{\text{outbord}_{IS}} - y_{\text{inbord}_{IS}}) \quad IS = 1, 2, \dots, NSS \quad (\text{Eqn.2.10})$$

The total forces acting on the blade are derived from the total velocity components at the blade together with control inputs. Inertial forces are neglected

because of little contribution to flight mechanics. Velocities components are made up of body velocities, the rotor own downwash and blade motion.

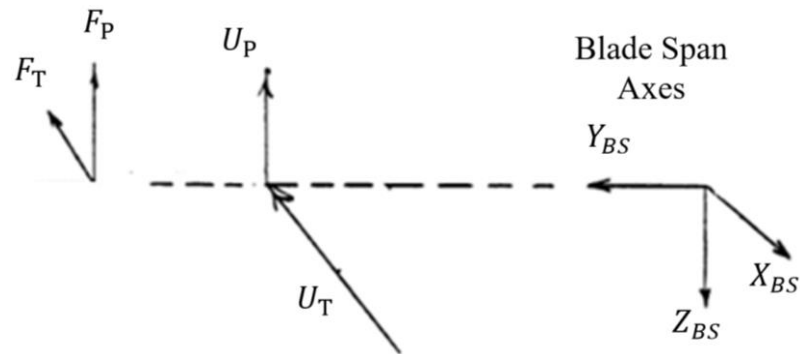


Figure 2.3: Velocity and force components of blade segment [5].

where “BS” means; blade segment.

Before calculations at the blade segment can be executed, several axes transformations must be implemented. Initially body axis angular and translational accelerations and velocities are transferred to the rotor hub and rotated through the shaft inclination angles  $I_\theta$  and  $I_\phi$  which are shaft tilt angles. The coordinate systems are given in the figure 2.4 and figure 2.5.

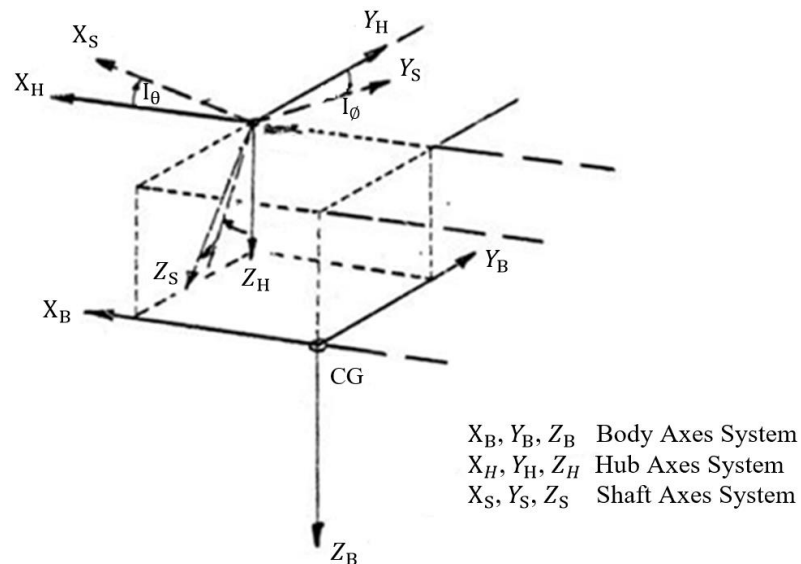
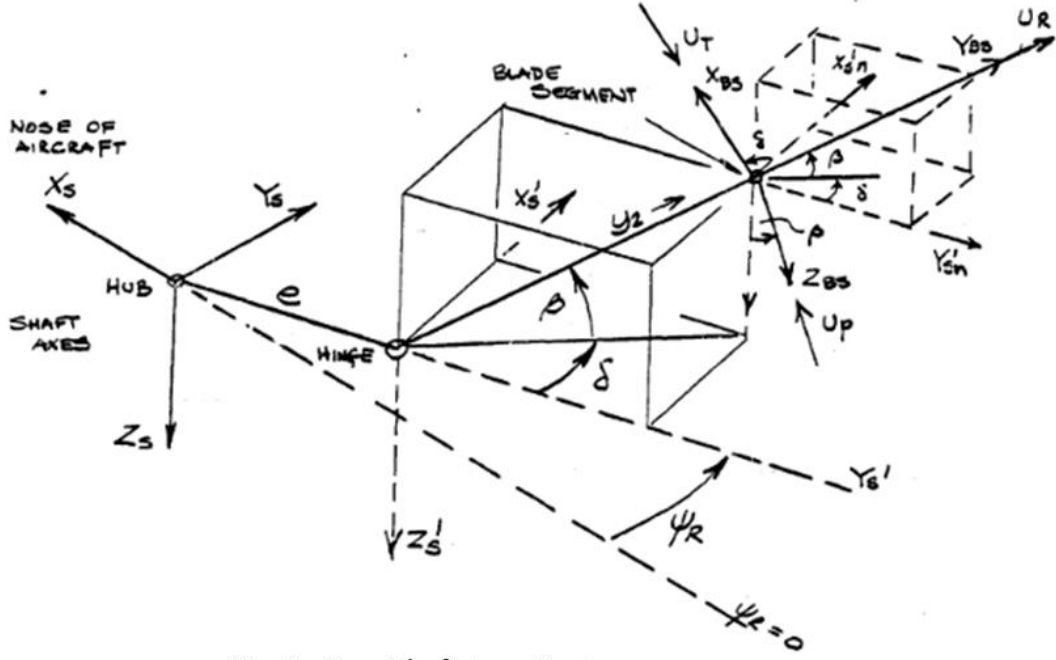


Figure 2.4: Body to shaft axes transformation [5].

where the body rates and body translational velocities are transferred through the rotor hub and by using shaft tilt angles transformation done for shaft axes.



$X_S, Y_S, Z_S$  Shaft Axes System  
 $X_S', Y_S', Z_S'$  Rotating Shaft Axes System  
 $X_{BS}, Y_{BS}, Z_{BS}$  Blade Span Axes System  
 $U_T, U_R, U_P$  Blade Element Velocities Along  
 $X_{BS}, Y_{BS}, Z_{BS}$  Respectively  
 $\beta$  and  $\delta$  are Euler Angles with  $\delta$  Rotating about  
 $Z_S'$  then  $\beta$  Rotating about  $X_{BS}$

Figure 2.5: Shaft axes to blade span axes transformations [5].

By using  $V = \dot{r} + w \times r$  and differentiating the equation for acceleration translational accelerations at the rotor hub becomes,

$$\begin{aligned} \dot{U}_{Hub} = \dot{U}_{Body} - rV_{Body} + qw_{Body} - X_H(q^2 + r^2) + Y_H(pq - \dot{r}) \\ + Z_H(pr + \dot{q}) + g_x \end{aligned} \quad (\text{Eqn.2.11})$$

$$\begin{aligned} \dot{V}_{Hub} = \dot{V}_{Body} - pV_{Body} + rU_{Body} + X_H(pq + \dot{r}) - Y_H(p^2 + r^2) \\ + Z_H(qr - \dot{p}) + g_y \end{aligned} \quad (\text{Eqn.2.12})$$

$$\begin{aligned} \dot{W}_{Hub} = \dot{W}_{Body} - pV_{Body} - qU_{Body} + X_H(pr + \dot{q}) + Y_H(qr + \dot{p}) \\ - Z_H(p^2 + q^2) + g_z \end{aligned} \quad (\text{Eqn.2.13})$$

where  $g$  components are gravity components and  $X_H, Y_H, Z_H$  are longitudinal, lateral and vertical rotor arms from the CG of the aircraft.



The translational velocities of the rotor hub can be written as

$$\mu_{XH} = \frac{1}{\Omega_T R_T} \{U_{Body} + qZ_H - rY_H\} \quad (\text{Eqn.2.14})$$

$$\mu_{YH} = \frac{1}{\Omega_T R_T} \{V_{Body} + rX_H - pZ_H\} \quad (\text{Eqn.2.15})$$

$$\mu_{ZH} = \frac{1}{\Omega_T R_T} \{w_{Body} - qX_H + pY_H\} \quad (\text{Eqn.2.16})$$

where  $X_H$ ,  $Y_H$ ,  $Z_H$  are longitudinal, lateral and vertical rotor arms from the CG of the aircraft. Velocity components are normalized by the tip speed of the blades (Advance ratio). These velocity components and body rates has to be transferred through the shaft axis.

Body to shaft axes transformation matrix is

$$A_{BDSH} = \begin{bmatrix} \cos I_\theta & 0 & -\sin I_\theta \\ \sin I_\theta \sin I_\phi & \cos I_\phi & \cos I_\theta \sin I_\phi \\ \sin I_\theta \cos I_\phi & -\sin I_\phi & \cos I_\theta \cos I_\phi \end{bmatrix} \quad (\text{Eqn.2.17})$$

Body translational accelerations at the hub (Shaft axes)

$$\begin{bmatrix} \dot{V}_{XS} \\ \dot{V}_{YS} \\ \dot{V}_{ZS} \end{bmatrix} = A_{BDSH} \begin{bmatrix} \dot{U}_{Hub} \\ \dot{V}_{Hub} \\ \dot{W}_{Hub} \end{bmatrix} \quad (\text{Eqn.2.18})$$

Body angular accelerations at the rotor hub (shaft axes)

$$\begin{bmatrix} \dot{p}_s \\ \dot{q}_s \\ \dot{r}_s \end{bmatrix} = A_{BDSH} \begin{bmatrix} \dot{p} \\ \dot{q} \\ \dot{r} \end{bmatrix} \quad (\text{Eqn.2.19})$$

Body translational velocities at the hub (Shaft axes)

$$\begin{bmatrix} \mu_{XS} \\ \mu_{YS} \\ \mu_{ZS} \end{bmatrix} = A_{BDSH} \begin{bmatrix} \mu_{XH} \\ \mu_{YH} \\ \mu_{ZH} \end{bmatrix} \quad (\text{Eqn.2.20})$$

Body angular velocities at the rotor hub (shaft axes)

$$\begin{bmatrix} p_s \\ q_s \\ r_s \end{bmatrix} = A_{BDSH} \begin{bmatrix} p \\ q \\ r \end{bmatrix} \quad (\text{Eqn.2.21})$$

The rotor air mass degree of freedom is primarily based on a uniform downwash distribution developed from rotor thrust by application of momentum theory. This uniform downwash which is passed through a first order lag is modified to account for the changing distribution with forward speed and aerodynamic pitching and rolling moment loading on the rotor. In the first case the resultant

uniform downwash is distributed 1st harmonically around the azimuth as a cosine function depending on the inclination of the rotor wake. So total downwash contribution at the rotor disk  $U_{PD}$  becomes,

$$\begin{aligned}
U_{PD_I} = & -D_{W0} \cos(\beta_{IB}) \\
& + (D_{WC} \\
& - K_{1X}D_{W0}) \cos(\beta_{IB}) [e \cos(\psi_{IB}) \\
& + y_{2IS} \cos(\psi_{IB} + \delta_{IB})] + (D_{WS} \\
& + K_{1Y}D_{W0}) \cos(\beta_{IB}) [e \sin(\psi_{IB}) \\
& + y_{2IS} \sin(\psi_{IB} + \delta_{IB})]
\end{aligned} \tag{Eqn.2.22}$$

where  $D_{W0}$  is the uniform downwash and obtained by using the momentum theory which is shown like,

$$D_{W0} = \frac{C_{TA}}{2\mu_{TOT}} \tag{Eqn.2.23}$$

where  $C_{TA}$  is the thrust coefficient and firstly estimated by using weight and  $\mu_{TOT}$  total velocity at the shaft axes and represented as,

$$\mu_{TOT} = \sqrt{\mu_{XS} + \mu_{YS} + \lambda_0} \tag{Eqn.2.24}$$

And  $\lambda_0$  is uniform inflow ratio (normalized induced velocity) calculated with momentum theory like,

$$\lambda_0 = \mu_{ZS} - D_{W0} \tag{Eqn.2.25}$$

$D_{WC}$  and  $D_{WS}$  are cosine and sine component of downwash which,

$$D_{WC} = \frac{C_{MHA}}{\mu_{TOT}} \tag{Eqn.2.26}$$

$$D_{WS} = \frac{C_{LHA}}{\mu_{TOT}} \tag{Eqn.2.27}$$

where  $C_{MHA}$  and  $C_{LHA}$  are pitch moment and rolling moment coefficients added through the uniform downwash and firstly estimated by using momentum theory and weight again like thrust coefficient  $C_{TA}$ .

First estimations;

$$C_{TA} = \frac{mg}{\rho\pi\Omega^2 R_T^4} \quad (\text{Eqn.2.28})$$

$$C_{MHA} = \frac{mg \sin(\beta_{1C})Z_H}{\rho\pi\Omega^2 R_T^5} \quad (\text{Eqn.2.29})$$

$$C_{LHA} = \frac{mg \sin(\beta_{1S})Z_H}{\rho\pi\Omega^2 R_T^5} \quad (\text{Eqn.2.30})$$

Other steps of iteration;

$$C_{TA} = \frac{T_{HA}}{\rho\pi\Omega^2 R_T^4} \quad (\text{Eqn.2.31})$$

$$C_{MHA} = \frac{M_{HA}}{\rho\pi\Omega^2 R_T^5} \quad (\text{Eqn.2.32})$$

$$C_{LHA} = \frac{L_{HA}}{\rho\pi\Omega^2 R_T^5} \quad (\text{Eqn.2.33})$$

So  $K_{1X}$  and  $K_{1Y}$  which are Glauert downwash factors and calculated with equations below,

$$K_{1X} = \frac{(\sqrt{\mu_{XS}^2 + \mu_{YS}^2})\mu_{XS}}{\mu_{TOT}^2} \quad (\text{Eqn.2.34})$$

$$K_{1Y} = \frac{(\sqrt{\mu_{XS}^2 + \mu_{YS}^2})\mu_{YS}}{\mu_{TOT}^2} \quad (\text{Eqn.2.35})$$

The blade segment total velocity components are developed in three parts. Those independent of segment position, those dependent on segment position and interference effects made up of downwash. The velocities at the blade segments are obtained by transforming the fixed shaft vectors into the rotating hub axes system then transferring to the blade hinge position, transforming into blade span axes through the euler angles flapping “ $\beta$ ” and lagging “ $\delta$ ” and finally transferring to the segment position on the blade. These total velocity components are used to calculate the resultant velocity, local mach number and local angle of attack which last two are need to be assigned for look-up table of blade airfoil aerodynamic coefficients (for  $C_l$  and  $C_d$  interpolation depends on mach number and angle of attack).

Total blade segment velocities in perpendicular direction will be,

$$U_{P_I} = U_{PA_{IB}} + \frac{y_{2IS}}{\Omega_T} (U_{PB_{IB}}) + U_{PD_I} \quad (\text{Eqn.2.36})$$

where  $I = 1, 2, \dots \dots \dots \text{NSS} * \text{NBS}$  total number of segments and  $IB = 1, 2, \dots \dots \text{NBS}$

The first velocity component which is independent of segment position is,

$$\begin{aligned} U_{PA_{IB}} = & -\mu_{XS} \sin(\beta_{IB}) \cos(\psi_{IB} + \delta_{IB}) \\ & + \mu_{YS} \sin(\beta_{IB}) \sin(\psi_{IB} + \delta_{IB}) + \mu_{ZS} \cos(\beta_{IB}) \\ & + \frac{e}{\Omega_T} \{ \cos(\beta_{IB}) [q_s \cos(\psi_{IB}) + p_s \sin(\psi_{IB})] \\ & - \sin(\beta_{IB}) \sin(\delta_{IB}) (r_s - \Omega) \} \end{aligned} \quad (\text{Eqn.2.37})$$

And second velocity component which is dependent of segment position is,

$$U_{PB_{IB}} = -\dot{\beta}_{IB} + q_s \cos(\psi_{IB} + \delta_{IB}) + p_s \sin(\psi_{IB} + \delta_{IB}) \quad (\text{Eqn.2.38})$$

For tangential direction total segment velocities will be,

$$U_{T_I} = U_{TA_{IB}} + \frac{y_{2IS}}{\Omega_T} (U_{TB_{IB}}) \quad (\text{Eqn.2.39})$$

$$\begin{aligned} U_{TA_{IB}} = & \mu_{XS} \sin(\psi_{IB} + \delta_{IB}) + \mu_{YS} \cos(\psi_{IB} + \delta_{IB}) \\ & - \frac{e}{\Omega_T} [\cos(\delta_{IB}) (r_s - \Omega)] \end{aligned} \quad (\text{Eqn.2.40})$$

$$\begin{aligned} U_{TB_{IB}} = & \dot{\delta}_{IB} \cos(\beta_{IB}) \\ & + \sin(\beta_{IB}) [p_s \cos(\psi_{IB} + \delta_{IB}) \\ & - q_s \sin(\psi_{IB} + \delta_{IB})] - \cos(\delta_{IB}) (r_s - \Omega) \end{aligned} \quad (\text{Eqn.2.41})$$

Finally resultant velocity at the blade segment will be,

$$U_{Y_I} = \sqrt{U_{T_I}^2 + U_{P_I}^2} \quad (\text{Eqn.2.42})$$

And Mach number

$$M = U_{Y_I} \frac{\Omega_T R_T}{a} \quad (\text{Eqn.2.43})$$

where “a” is the speed of sound.

After obtaining the velocity components and by velocity terms determining the Mach number and angle of attack for look up table the aero data can be defined and interpolated so next step should be calculating rotor aero forces and moments. So blade segment forces in blade span axis will be,

$$F_{P_I} = \frac{1}{2} \rho \Omega^2 R_T^3 (C_{y_{IS}} \Delta y_{IS}) U_{Y_I} \{C_{l_I} U_{T_I} + C_{d_I} U_{P_I}\} \quad (\text{Eqn.2.44})$$

$$F_{T_I} = \frac{1}{2} \rho \Omega^2 R_T^3 (C_{y_{IS}} \Delta y_{IS}) U_{Y_I} \{C_{d_I} U_{T_I} + C_{l_I} U_{P_I}\} \quad (\text{Eqn.2.45})$$

So aerodynamic forces in blade span axes per blade becomes,

$$F_{PB_{IB}} = \sum_{IS=1}^{NSS} F_{P_I} \quad (\text{Eqn.2.46})$$

$$F_{TB_{IB}} = \sum_{IS=1}^{NSS} F_{T_I} \quad (\text{Eqn.2.47})$$

As a result aerodynamic moments about the hinge in blade span axes (per blade),

$$M_{FAB_{IB}} = R_T \sum_{IS=1}^{NSS} y_{2IS} F_{P_I} \quad (\text{flapping}) \quad (\text{Eqn.2.48})$$

$$M_{LAB_{IB}} = R_T \sum_{IS=1}^{NSS} y_{2IS} F_{T_I} \quad (\text{lagging}) \quad (\text{Eqn.2.49})$$

Aerodynamic moments about the hinge (flapping component is dominant so only flapping moment will considered) at the fixed shaft axes for 1st harmonics inflow

$$L_{HA} = -\frac{b}{b_s} \sum_{IB=1}^{NBS} M_{FAB_{IB}} \sin(\psi_{IB} + \delta_{IB}) \quad (\text{Eqn.2.50})$$

$$M_{HA} = -\frac{b}{b_s} \sum_{IB=1}^{NBS} M_{FAB_{IB}} \cos(\psi_{IB} + \delta_{IB}) \quad (\text{Eqn.2.51})$$

where “b” is total number of blades and “b<sub>s</sub>” is the number of azimuthally separated locations for average technique of calculation total moments on the TPP. If the per blade forces in blade span axes are transferred to rotating shaft axes,

$$F_{XA_{IB}} = -F_{TB_{IB}} \cos(\delta_{IB}) - F_{PB_{IB}} \sin(\beta_{IB}) \sin(\delta_{IB}) \quad (\text{Eqn.2.52})$$

$$F_{YA_{IB}} = F_{TB_{IB}} \sin(\delta_{IB}) - F_{PB_{IB}} \sin(\beta_{IB}) \cos(\delta_{IB}) \quad (\text{Eqn.2.53})$$

$$F_{ZA_{IB}} = F_{PB_{IB}} \cos(\beta_{IB}) \quad (\text{Eqn.2.54})$$

Aerodynamic thrust component for derivation of uniform inflow component should be,

$$T_{HA} = -\frac{b}{b_s} \sum_{IB=1}^{NBS} F_{ZA_{IB}} \quad (\text{Eqn.2.55})$$

To reflect the ground effect Cheeseman & Bennett ground effect formula is used [15]:

$$\frac{T_{IGE}}{T_{OGE}} = k_G = \frac{1}{1 - \frac{1}{16} \left(\frac{R_T}{z}\right)^2 \left[ \frac{1}{1 + \left(\frac{V}{v}\right)^2} \right]} \quad (\text{Eqn.2.56})$$

where ,V is the airspeed velocity and v is the velocity induced by the rotor normal to the disk. z is the rotor hub height from ground. Considering the ground effect, the total main rotor thrust become:

$$T_{HA} = k_G T_{HA} \quad (\text{Eqn.2.57})$$

Finally the flapping and lagging dynamic equations should be added for obtaining Euler angles of main rotor. The flapping and lagging equation of motion of main rotor becomes,

$$\begin{aligned}
\ddot{\beta}_{IB} = & \frac{M_b}{I_b} \left[ \cos(\beta_{IB}) \{ \dot{W}_{SH} \right. \\
& + eR_T [2\Omega(p_s \cos(\psi_{IB}) - q_s \sin(\psi_{IB})) + \dot{p}_s \sin(\psi_{IB}) \\
& + \dot{q}_s \cos(\psi_{IB})] \} \\
& + \sin(\beta_{IB}) \cos(\delta_{IB}) \{ \dot{V}_s \sin(\psi_{IB}) - \dot{U}_s \cos(\psi_{IB}) \\
& - e(r_s - \Omega)^2 \} \left. \right] \\
& + \cos(\beta_{IB})^2 \left[ \cos(\delta_{IB}) \{ \dot{p}_s \sin(\psi_{IB}) + \dot{q}_s \cos(\psi_{IB}) \right. \\
& - 2(\dot{\delta}_{IB} + \Omega)(q_s \sin(\psi_{IB}) - p_s \cos(\psi_{IB})) \} \\
& - 2\Omega \sin(\delta_{IB}) (p_s \sin(\psi_{IB}) - q_s \cos(\psi_{IB})) \left. \right] \\
& + \sin(\beta_{IB}) \cos(\beta_{IB}) [2\dot{\delta}_{IB}(r_s - \Omega) - (r_s - \Omega)^2] \\
& + \frac{M_{FAB_{IB}}}{I_b}
\end{aligned} \tag{Eqn.2.58}$$

$$\begin{aligned}
\ddot{\delta}_{IB} = & \frac{M_b}{I_b \cos(\beta_{IB})} \left[ \sin(\beta_{IB}) \{ \dot{V}_s \sin(\psi_{IB}) - \dot{U}_s \cos(\psi_{IB}) - e(r_s - \Omega)^2 \} \right. \\
& - \cos(\delta_{IB}) \{ \dot{U}_s \sin(\psi_{IB}) + \dot{V}_s \cos(\psi_{IB}) + e(\dot{\Omega} - \dot{r}_s) \} \left. \right] \\
& + \frac{\sin(\beta_{IB})}{\cos(\beta_{IB})} [2\dot{\beta}_{IB}(\Omega + \dot{\delta}_{IB} - r_s) + \dot{q}_s \sin(\psi_{IB} + \delta_{IB}) \\
& - \dot{p}_s \cos(\psi_{IB} + \delta_{IB})] + (\dot{r}_s - \dot{\Omega}) \\
& + 2\dot{\beta}_{IB} [\cos(\delta_{IB}) \{ q_s \sin(\psi_{IB}) - p_s \cos(\psi_{IB}) \} \\
& + \sin(\delta_{IB}) \{ p_s \sin(\psi_{IB}) + q_s \cos(\psi_{IB}) \}] \\
& - \frac{M_{LAB_{IB}}}{I_b \cos(\beta_{IB})}
\end{aligned} \tag{Eqn.2.59}$$

As it can be easily seen that all pitch, roll and yaw rates are added through the dynamic equations and inertial forces can be obtained by Euler acceleration but as mentioned before inertial forces contributions on the flight mechanics are negligible.

So under these circumstances total forces and moments about the hub fixed shaft axes becomes.

$$T_H = -\frac{b}{b_s} \sum_{IB=1}^{NBS} F_{ZA_{IB}} \quad (\text{Eqn.2.60})$$

$$H_H = \frac{b}{b_s} \sum_{IB=1}^{NBS} \{F_{YA_{IB}} \cos(\psi_{IB}) - F_{XA_{IB}} \sin(\psi_{IB})\} \quad (\text{Eqn.2.61})$$

$$J_H = -\frac{b}{b_s} \sum_{IB=1}^{NBS} \{F_{XA_{IB}} \cos(\psi_{IB}) - F_{YA_{IB}} \sin(\psi_{IB})\} \quad (\text{Eqn.2.62})$$

$$M_H = \frac{b}{b_s} \sum_{IB=1}^{NBS} e * F_{ZA_{IB}} * \cos(\psi_{IB}) \quad (\text{Eqn.2.63})$$

$$L_H = \frac{b}{b_s} \sum_{IB=1}^{NBS} e * F_{ZA_{IB}} * \sin(\psi_{IB}) \quad (\text{Eqn.2.64})$$

$$Q_H = -\frac{b}{b_s} \sum_{IB=1}^{NBS} \{e * F_{XA_{IB}} - M_{LAB_{IB}} \cos(\beta_{IB})\} \quad (\text{Eqn.2.65})$$

These forces and moment about the hub fixed shaft axes are transformed to body axes and forces are transferred to center of gravity of helicopter.

$$[A_{SHBD}] = [A_{BDSH}]^T \quad (\text{Eqn.2.66})$$

$$\begin{bmatrix} X_{MR} \\ Y_{MR} \\ Z_{MR} \end{bmatrix} = A_{SHBD} \begin{bmatrix} -H_H \\ -J_H \\ -T_H \end{bmatrix} \quad (\text{Eqn.2.67})$$

$$\begin{bmatrix} L_{MR} \\ M_{MR} \\ N_{MR} \end{bmatrix} = A_{SHBD} \begin{bmatrix} L_H \\ M_H \\ Q_H \end{bmatrix} + \begin{bmatrix} Y_H Z_{MR} - Z_H Y_{MR} \\ Z_H X_{MR} - X_H Z_{MR} \\ X_H Y_{MR} - Y_H X_{MR} \end{bmatrix} \quad (\text{Eqn.2.68})$$



### 2.3 Tail Rotor Model Theory

Tail rotor model is based on GEN-HEL. Main rotor-tail rotor and fuselage-tail rotor interference effect is reflected by interference tables in GEN-HEL.

Tail rotor model mathematical formulations are given below:

Tail rotor moment arms in three directions are computed;

$$F_{TR} = FS_{TR} - FS_{CGB} \quad (\text{Eqn.2.69})$$

$$W_{TR} = WL_{TR} - WL_{CGB} \quad (\text{Eqn.2.70})$$

$$B_{TR} = BL_{TR} - BL_{CGB} \quad (\text{Eqn.2.71})$$

Total interference velocities are;

$$V_{XITR} = V_{XMRTR} \quad (\text{Eqn.2.72})$$

$$V_{YITR} = V_{YMRTR} + V_{YWFTR} \quad (\text{Eqn.2.73})$$

$$V_{ZITR} = V_{ZMRTR} + V_{ZWFTR} \quad (\text{Eqn.2.74})$$

where  $V_{XMRTR}$ ,  $V_{YMRTR}$ ,  $V_{ZMRTR}$  are main rotor-tail rotor interference velocities and  $V_{YWFTR}$  and  $V_{ZWFTR}$  are fuselage-tail rotor interference velocities. These velocities are determined by interference tables in GEN-HEL.

Local velocity components at the tail rotor are calculated in the body axes.

$$V_{XTRB} = (V_{Xb} + V_{XgTR})K_{QTR} - qW_{TR} + rB_{TR} + V_{XITR} \quad (\text{Eqn.2.75})$$

$$V_{YTRB} = (V_{Yb} + V_{YgTR})K_{QTR} + pW_{TR} - rF_{TR} + V_{YITR} \quad (\text{Eqn.2.76})$$

$$V_{ZTRB} = (V_{Zb} + V_{ZgTR})K_{QTR} + qF_{TR} - pB_{TR} + V_{ZITR} \quad (\text{Eqn.2.77})$$

where  $V_{XgTR}$ ,  $V_{YgTR}$ ,  $V_{ZgTR}$  are gust velocities and  $K_{QTR}$  is square root of dynamic pressure ratio explained at GEN-HEL. Tail rotor velocities in the body axes are transformed to shaft axes to find shaft axes total velocities;

$$V_{XTR} = V_{XTRB} \quad (\text{Eqn.2.78})$$

$$V_{YTR} = V_{YTRB}\cos\Gamma_{TR} + V_{ZTRB}\sin\Gamma_{TR} \quad (\text{Eqn.2.79})$$

$$V_{ZTR} = -V_{YTRB}\sin\Gamma_{TR} + V_{ZTRB}\cos\Gamma_{TR} \quad (\text{Eqn.2.80})$$

where  $\Gamma_{TR}$  is the cant angle of tail rotor described in GEN-HEL.

Shaft axes velocities normalized by rotor tip speed;

$$\mu_{XTR} = V_{XTR}/(\Omega R)_{TR} \quad (\text{Eqn.2.81})$$

$$\mu_{YTR} = V_{YTR}/(\Omega R)_{TR} \quad (\text{Eqn.2.82})$$

$$\mu_{ZTR} = V_{ZTR}/(\Omega R)_{TR} \quad (\text{Eqn.2.83})$$

$$\mu_{TR} = \sqrt{\mu_{XTR}^2 + \mu_{YTR}^2} \quad (\text{Eqn.2.84})$$

Bailey Coefficients are given below;

$$t_{3.1} = \frac{B^2}{2} + \frac{\mu_{TR}^2}{4} \quad (\text{Eqn.2.85})$$

$$t_{3.2} = \frac{B^3}{3} + \frac{B}{2}\mu_{TR}^2 \quad (\text{Eqn.2.86})$$

$$t_{3.3} = \frac{B^4}{4} + \frac{B^2}{4}\mu_{TR}^2 \quad (\text{Eqn.2.87})$$

$$G = \frac{A_{TR}}{2} + \left[ \frac{bc}{\pi R} \right]_{TR} \quad (\text{Eqn.2.88})$$

Additional coefficients are defined as below[6]:

$$t_{4.1} = \frac{B^2}{2} + \frac{5}{4} + \frac{\gamma^2 B^2}{1296} \mu_{TR}^2 \quad (\text{Eqn.2.89})$$

$$t_{4.2} = \frac{B^3}{3} + \frac{8B}{3} + \frac{\gamma^2 B^9}{864} \mu_{TR}^2 \quad (\text{Eqn.2.90})$$

$$t_{4.3} = \frac{B^4}{4} + 2B^2 + \frac{\gamma^2 B^{10}}{1080} \mu_{TR}^2 \quad (\text{Eqn.2.91})$$

$$t_{4.4} = \frac{8B^2}{9} + \frac{\gamma^2 B^{10}}{2304} \mu_{TR}^2 \quad (\text{Eqn.2.92})$$

$$t_{4.5} = \frac{4B^2}{3} + \frac{\gamma^2 B^{11}}{1440} \mu_{TR}^2 \quad (\text{Eqn.2.93})$$

$$t_{4.6} = \frac{B^4}{2} + \frac{\gamma^2 B^{12}}{3600} \mu_{TR}^2 \quad (\text{Eqn.2.94})$$

$$t_{5.1} = \frac{1}{4} + \frac{1}{4} \mu_{TR}^2 \quad (\text{Eqn.2.95})$$

$$t_{5.2} = \frac{1}{3} \quad (\text{Eqn.2.96})$$

$$t_{5.3} = \frac{1}{4} + \frac{1}{4} \mu_{TR}^2 \quad (\text{Eqn.2.97})$$

$$t_{5.4} = \frac{1}{5} + \frac{1}{6} \mu_{TR}^2 \quad (\text{Eqn.2.98})$$

$$t_{5.5} = \frac{1}{2} - \frac{1}{4} + \frac{1}{B^2} + \frac{1}{2B^4} + \frac{\gamma^2 B^4}{162} - \frac{B^5}{81} + \frac{B^6}{144} \mu_{TR}^2 \quad (\text{Eqn.2.99})$$

$$t_{5.6} = \frac{2}{3} + \frac{4}{3B} + \frac{4}{3B^3} + \frac{\gamma^2 B^5}{108} - \frac{B^6}{54} + \frac{B^7}{96} \mu_{TR}^2 \quad (\text{Eqn.2.100})$$

$$t_{5.7} = \frac{1}{2} + 1 + \frac{1}{B^2} + \frac{\gamma^2 B^6}{135} - \frac{2B^7}{135} + \frac{B^8}{120} \mu_{TR}^2 \quad (\text{Eqn.2.101})$$

$$t_{5.8} = \frac{1}{4} + \frac{1}{4} + \frac{8}{9B^2} + \frac{\gamma^2 B^6}{288} - \frac{B^7}{144} + \frac{B^8}{256} \mu_{TR}^2 \quad (\text{Eqn.2.102})$$

$$t_{5.9} = \frac{2}{5} + \frac{1}{3} + \frac{4}{3B} + \frac{\gamma^2 B^7}{180} - \frac{B^8}{90} + \frac{B^9}{160} \mu_{TR}^2 \quad (\text{Eqn.2.103})$$

$$t_{5.10} = \frac{1}{6} + \frac{5}{8} + \frac{\gamma^2 B^8}{450} - \frac{B^9}{225} + \frac{B^{10}}{400} \mu_{TR}^2 \quad (\text{Eqn.2.104})$$

for which

$$\gamma = \frac{\rho a_{TR} C_{TR} R_{TR}^4}{I_{B_{TR}}} \quad (\text{Eqn.2.105})$$

The tail rotor torque coefficient is computed as;

$$\begin{aligned} CQ_{TR} = \frac{\sigma}{2} [ & (\delta_2 t_{5.5} - a_{TR} t_{4.1}) \lambda^2 + (\delta_2 t_{5.6} - a_{TR} t_{4.2}) \theta_{TR} \lambda \\ & + (\delta_2 t_{5.7} - a_{TR} t_{4.3}) \theta_1 \lambda \\ & + (\delta_2 t_{5.8} - a_{TR} t_{4.4}) \theta_{TR}^2 \\ & + (\delta_2 t_{5.9} - a_{TR} t_{4.5}) \theta_1 \theta_{TR} \\ & + (\delta_2 t_{5.10} - a_{TR} t_{4.6}) \theta_1^2 + \delta_0 t_{5.1} + \delta_1 t_{5.2} \lambda \\ & + \delta_1 t_{5.3} \theta_{TR} + \delta_1 t_{5.4} \theta_1 ] \end{aligned} \quad (\text{Eqn.2.106})$$

where  $\sigma = \frac{bc}{\pi R_{TR}}$  and  $\theta_1 = T_{WSTTR}/57.3$ . Tail rotor torque is then computed as

$$Q_{TR} = CQ_{TR} * \pi \rho \Omega_{TR}^2 R_{TR}^5 * OMGBX^2 \quad (\text{Eqn.2.107})$$

Tail rotor blade pitch angle is calculated;

$$\theta_{TR} = \frac{1}{57.3} \left[ \theta_{TTR} - T_{TR(t-1)} \left( \frac{\partial a_0}{\partial T_{TR}} \right) \tan \delta_3 + B_{IASTR} \right] \quad (\text{Eqn.2.108})$$

where  $\theta_{TTR}$  is tail rotor commanded blade pitch,  $T_{TR(t-1)}$  is tail rotor thrust of previous time step,  $\left( \frac{\partial a_0}{\partial T_{TR}} \right)$  is rate of change of coning with thrust,  $\delta_3$  is flapping hinge offset angle and  $B_{IASTR}$  is blade pitch correction to linear twist.

Tail Rotor Inflow is calculated as follows;

$$D_{WSHTR(t)} = \frac{G \left[ \mu_{ZTR}(t_{3.1}) + \theta_{TR}(t_{3.2}) + \frac{T_{WSTTR}}{57.3}(t_{3.3}) \right]}{2 \sqrt{\mu_{TR}^2 + \lambda_{TR_{t-1}}^2} + G(t_{3.1})} \quad (\text{Eqn.2.109})$$

$$\lambda_{TR_t} = \mu_{ZTR} - D_{WSHTR(t)} \quad (\text{Eqn.2.110})$$

where  $T_{WSTTR}$  is tail rotor linear blade twist.

Tail rotor thrust is computed as follows;

$$T_{TR} = 2\rho\pi R_{TR}^4 D_{WSHTR(t)} \sqrt{\mu_{TR}^2 + \lambda_{TR_t}^2} \Omega_{TR}^2 K_{BLKTR} \quad (\text{Eqn.2.111})$$

where  $K_{BLKTR}$  is the vertical tail blockage factor described in GEN-HEL.

Finally tail rotor forces and moments at the CG in body axes is obtained;

$$X_{TR} = -\frac{1}{2} \rho C_{DTR} V_{XTR}^2 \quad (\text{Eqn.2.112})$$

$$Y_{TR} = T_{TR} \sin \Gamma_{TR} \quad (\text{Eqn.2.113})$$

$$Z_{TR} = -T_{TR} \cos \Gamma_{TR} \quad (\text{Eqn.2.114})$$

$$L_{TR} = Y_{TR} W_{TR} - Z_{TR} B_{TR} \quad (\text{Eqn.2.115})$$

$$M_{TR} = Z_{TR} F_{TR} - X_{TR} W_{TR} + Q_{TR} \sin(\Gamma_{TR}) \quad (\text{Eqn.2.116})$$

$$N_{TR} = X_{TR} B_{TR} - Y_{TR} F_{TR} - Q_{TR} \cos(\Gamma_{TR}) \quad (\text{Eqn.2.117})$$

## 2.4 Fuselage Model Theory

Fuselages of helicopters has generally arbitrary geometric shapes. To reach high fidelity fuselage mathematical model, aerodynamic coefficient tables are needed. It is hard to develop high fidelity generic fuselage mathematical model without aerodynamic coefficient tables. In minimum complexity helicopter model[7], there is an approach for generic fuselage model. In this model, quadratic force coefficients are used to calculate the fuselage forces. Fuselage is modelled as a virtual flat plate areas which is not creating lift, but creating only drag. These areas are used in force equations as drag coefficients in three directions in body frame. Fuselage moments are obtained by carrying the calculated fuselage forces to center of gravity. For a helicopter, if there is not fuselage aerodynamic coefficient data, this model can be used.

In this study, to develop higher fidelity fuselage model, blackhawk fuselage aerodynamic force and moment coefficient tables in GEN-HEL are used.

Fuselage model is based on GEN-HEL and equations are given below:

The velocity components acting on the fuselage in its local body axes system are as follows.

$$V_{XWF} = V_{Xb} + V_{XgWF} + V_{XIWF} \quad (\text{Eqn.2.118})$$

$$V_{YWF} = V_{Yb} + V_{YgWF} + V_{YIWF} \quad (\text{Eqn.2.119})$$

$$V_{ZWF} = V_{Zb} + V_{ZgWF} + V_{ZIWF} \quad (\text{Eqn.2.120})$$

where  $V_{XgWF}$ ,  $V_{YgWF}$ ,  $V_{ZgWF}$  are the gust velocities,  $V_{Xb}$ ,  $V_{Yb}$ ,  $V_{Zb}$  are helicopter body velocities and  $V_{XIWF}$ ,  $V_{YIWF}$ ,  $V_{ZIWF}$  are main rotor wash interference velocities on fuselage. From fuselage velocity components, fuselage angle of attack ( $\alpha_{WF}$ ), sideslip angle ( $\beta_{WF}$ ) and dynamic pressure ( $Q_{WF}$ ) is calculated.

$$\alpha_{WF} = \tan^{-1} \left( \frac{V_{ZWF}}{|V_{XWF}|} \right) \quad (\text{Eqn.2.121})$$

$$\beta_{WF} = \tan^{-1} \left( \frac{V_{YWF}}{\sqrt{V_{XWF}^2 + V_{ZWF}^2}} \right) \quad (\text{Eqn.2.122})$$

$$Q_{WF} = \frac{1}{2} \rho (V_{XWF}^2 + V_{YWF}^2 + V_{ZWF}^2) \quad (\text{Eqn.2.123})$$

DQFTOT, YQFTOT, LQFTOT, RQFTOT, MQFTOT, NQFTOT are fuselage aerodynamic loading coefficients and found by using  $\alpha_{WF}$ ,  $\beta_{WF}$ ,  $Q_{WF}$  and fuselage aerodynamic tables as explained in GEN-HEL.

Fuselage moment arms in three directions are computed;

$$F_{WT} = FS_{CGB} - FS_{WF} \quad (\text{Eqn.2.124})$$

$$W_{WT} = WL_{CGB} - WL_{WF} \quad (\text{Eqn.2.125})$$

$$B_{WT} = BL_{CGB} - BL_{WF} \quad (\text{Eqn.2.126})$$

Fuselage forces and moments in wind axis are determined by;

$$D_{FUS} = DQFTOT * Q_{WF} \quad (\text{Eqn.2.127})$$

$$Y_{FUS} = YQFTOT * Q_{WF} \quad (\text{Eqn.2.128})$$

$$L_{FUS} = LQFTOT * Q_{WF} \quad (\text{Eqn.2.129})$$

$$R_{FUS} = RQFTOT * Q_{WF} \quad (\text{Eqn.2.130})$$

$$M_{FUS} = MQFTOT * Q_{WF} \quad (\text{Eqn.2.131})$$

$$N_{FUS} = NQFTOT * Q_{WF} \quad (\text{Eqn.2.132})$$

Finally, these forces and moments in wind axis need to be transformed into body axes and forces need to be transferred to the center of gravity of helicopter.

$$\begin{bmatrix} X_{WF} \\ Y_{WF} \\ Z_{WF} \end{bmatrix} = \begin{bmatrix} \cos \alpha_{WF} \cos \beta_{WF} & \cos \alpha_{WF} \sin \beta_{WF} & -\sin \alpha_{WF} \\ \sin \beta_{WF} & -\cos \beta_{WF} & 0 \\ \sin \alpha_{WF} \cos \beta_{WF} & \sin \alpha_{WF} \sin \beta_{WF} & \cos \alpha_{WF} \end{bmatrix} \begin{bmatrix} -D_{FUS} \\ -Y_{FUS} \\ -L_{FUS} \end{bmatrix} \quad (\text{Eqn.2.133})$$

$$\begin{bmatrix} L_{WF} \\ M_{WF} \\ N_{WF} \end{bmatrix} = \begin{bmatrix} L_{WFWF} \\ M_{WFWF} \\ N_{WFWF} \end{bmatrix} + \begin{bmatrix} -Y_{WF}W_{WT} + Z_{WF}B_{WT} \\ -Z_{WF}F_{WT} + X_{WF}W_{WT} \\ +Y_{WF}F_{WT} - X_{WF}B_{WT} \end{bmatrix} \quad (\text{Eqn.2.134})$$

where

$$\begin{bmatrix} L_{WFWF} \\ M_{WFWF} \\ N_{WFWF} \end{bmatrix} = \begin{bmatrix} \cos \alpha_{WF} \cos \beta_{WF} & \cos \alpha_{WF} \sin \beta_{WF} & -\sin \alpha_{WF} \\ \sin \beta_{WF} & -\cos \beta_{WF} & 0 \\ \sin \alpha_{WF} \cos \beta_{WF} & \sin \alpha_{WF} \sin \beta_{WF} & \cos \alpha_{WF} \end{bmatrix} \begin{bmatrix} R_{FUS} \\ -M_{FUS} \\ N_{FUS} \end{bmatrix} \quad (\text{Eqn.2.135})$$

## 2.5 Horizontal Tail Model Theory

Horizontal tail model is based on GEN-HEL. Main rotor-horizontal tail and fuselage-horizontal tail interference effect is reflected by interference tables in GEN-HEL.

Horizontal tail model mathematical formulations are given below:

Horizontal tail moment arms in three directions are computed;

$$F_{HT1} = FS_{H1} - FS_{CGB} \quad (\text{Eqn.2.136})$$

$$W_{HT1} = WL_{H1} - WL_{CGB} \quad (\text{Eqn.2.137})$$

$$B_{HT1} = BL_{H1} - BL_{CGB} \quad (\text{Eqn.2.138})$$

Total interference velocities are;

$$V_{XIH1} = V_{XMRH1} \quad (\text{Eqn.2.139})$$

$$V_{YIH1} = V_{YMRH1} \quad (\text{Eqn.2.140})$$

$$V_{ZIH1} = V_{ZMRH1} + V_{ZWFH1} \quad (\text{Eqn.2.141})$$

where  $V_{XMRH1}$ ,  $V_{YMRH1}$ ,  $V_{ZMRH1}$  are main rotor-horizontal tail interference velocities and  $V_{ZWFH1}$  is fuselage-horizontal tail interference velocities. These velocities are determined by interference tables in GEN-HEL.

Local velocity components and dynamic pressure at the horizontal tail are calculated.

$$V_{XH1} = (V_{Xb} + V_{XgH1})K_{QH1} - qW_{HT1} + rB_{HT1} + V_{XH1} \quad (\text{Eqn.2.142})$$

$$V_{YH1} = (V_{Yb} + V_{YgH1})K_{QH1} + pW_{HT1} - rF_{HT1} + V_{YH1} \quad (\text{Eqn.2.143})$$

$$V_{ZH1} = (V_{Zb} + V_{ZgH1})K_{QH1} + qF_{HT1} - pB_{HT1} + V_{ZH1} \quad (\text{Eqn.2.144})$$

$$Q_{H1} = \frac{1}{2} \rho (V_{XH1}^2 + V_{YH1}^2 + V_{ZH1}^2) \quad (\text{Eqn.2.145})$$

where  $V_{XgH1}$ ,  $V_{YgH1}$ ,  $V_{ZgH1}$  are gust velocities and  $K_{QH1}$  is square root of dynamic pressure ratio explained at GEN-HEL. From horizontal tail velocity components, horizontal tail angle of attack ( $\alpha_{WF}$ ) and sideslip angle ( $\beta_{WF}$ ) are calculated.

$$\alpha_{HH1} = \tan^{-1} \left( \frac{V_{ZH1}}{|V_{XH1}|} \right) \quad (\text{Eqn.2.146})$$

$$\beta_{H1} = \tan^{-1} \left( \frac{V_{YH1}}{\sqrt{V_{XH1}^2 + V_{ZH1}^2}} \right) \quad (\text{Eqn.2.147})$$

Horizontal tail forces in wind axis are determined by;

$$D_{HT1} = Q_{H1} * S_{AH1} * C_{DH1} \quad (\text{Eqn.2.148})$$

$$Y_{HT1} = 0 \quad (\text{Eqn.2.149})$$

$$L_{HT1} = Q_{H1} * S_{AH1} * C_{LH1} \quad (\text{Eqn.2.150})$$

Finally, these forces in wind axis need to be transformed into body axes and transferred to the center of gravity of helicopter.

$$\begin{bmatrix} X_{H1} \\ Y_{H1} \\ Z_{H1} \end{bmatrix} = \begin{bmatrix} \cos \alpha_{H1} \cos \beta_{H1} & \cos \alpha_{H1} \sin \beta_{H1} & -\sin \alpha_{H1} \\ \sin \beta_{H1} & -\cos \beta_{H1} & 0 \\ \sin \alpha_{H1} \cos \beta_{H1} & \sin \alpha_{H1} \sin \beta_{H1} & \cos \alpha_{H1} \end{bmatrix} \begin{bmatrix} -D_{HT1} \\ -Y_{HT1} \\ -L_{HT1} \end{bmatrix} \quad (\text{Eqn.2.151})$$

$$\begin{bmatrix} L_{H1} \\ M_{H1} \\ N_{H1} \end{bmatrix} = \begin{bmatrix} Y_{H1} W_{HT1} - Z_{H1} B_{HT1} \\ -X_{H1} W_{HT1} + Z_{H1} F_{HT1} \\ -Y_{H1} F_{HT1} + X_{H1} B_{HT1} \end{bmatrix} \quad (\text{Eqn.2.152})$$

## 2.6 Vertical Tail Model Theory

Vertical tail model is based on GEN-HEL. Main rotor-vertical tail and fuselage-vertical tail interference effect is reflected by interference tables in GEN-HEL.

Vertical tail model mathematical formulations are given below:

Vertical tail moment arms in three directions are computed;

$$F_{VT1} = FS_{VT1} - FS_{CGB} \quad (\text{Eqn.2.153})$$

$$W_{VT1} = WL_{VT1} - WL_{CGB} \quad (\text{Eqn.2.154})$$

$$B_{VT1} = BL_{VT1} - BL_{CGB} \quad (\text{Eqn.2.155})$$

Total interference velocities are;

$$V_{XIV1} = V_{XMRV1} \quad (\text{Eqn.2.156})$$

$$V_{YIV1} = V_{YMRV1} + V_{YWV1} \quad (\text{Eqn.2.157})$$

$$V_{ZIV1} = V_{ZMRV1} \quad (\text{Eqn.2.158})$$

where  $V_{XMRV1}$ ,  $V_{YMRV1}$ ,  $V_{ZMRV1}$  are main rotor-vertical tail interference velocities and  $V_{YWV1}$  is fuselage-vertical tail interference velocities. These velocities are determined by interference tables in GEN-HEL.

Local velocity components and dynamic pressure at the vertical tail are calculated.

$$V_{XV1} = (V_{Xb} + V_{XgV1})K_{QV1} - qW_{VT1} + rB_{VT1} + V_{XIV1} \quad (\text{Eqn.2.159})$$

$$V_{YV1} = (V_{Yb} + V_{YgV1})K_{QV1} - rF_{VT1} + pW_{VT1} + V_{YIV1} \quad (\text{Eqn.2.160})$$

$$V_{ZV1} = (V_{Zb} + V_{ZgV1})K_{QV1} + qF_{VT1} - pB_{VT1} + V_{ZIV1} \quad (\text{Eqn.2.161})$$

$$Q_{V1} = \frac{1}{2} \rho (V_{XV1}^2 + V_{YV1}^2 + V_{ZV1}^2) \quad (\text{Eqn.2.162})$$

where  $V_{XgV1}$ ,  $V_{YgV1}$ ,  $V_{ZgV1}$  are gust velocities and  $K_{QV1}$  is square root of dynamic pressure ratio explained at GEN-HEL. From vertical tail velocity components, vertical tail angle of attack ( $\alpha_{VF}$ ) and sideslip angle ( $\beta_{VF}$ ) are calculated.

$$\alpha_{V1} = \tan^{-1} \left( \frac{V_{ZV1}}{|V_{XV1}|} \right) \quad (\text{Eqn.2.163})$$

$$\beta_{V1} = \tan^{-1} \left( \frac{V_{YV1}}{\sqrt{V_{XV1}^2 + V_{ZV1}^2}} \right) \quad (\text{Eqn.2.164})$$

Vertical tail forces in wind axis are determined by;

$$D_{VT1} = Q_{V1} * S_{AV1} * C_{DV1} \quad (\text{Eqn.2.165})$$

$$Y_{VT1} = Q_{V1} * S_{AV1} * C_{LV1} \quad (\text{Eqn.2.166})$$

$$L_{VT1} = 0 \quad (\text{Eqn.2.167})$$



Finally, these forces in wind axis need to be transformed into body axes and transferred to the center of gravity of helicopter.

$$\begin{bmatrix} X_{V1} \\ Y_{V1} \\ Z_{V1} \end{bmatrix} = \begin{bmatrix} \cos \alpha_{V1} \cos \beta_{V1} & \cos \alpha_{V1} \sin \beta_{V1} & -\sin \alpha_{V1} \\ \sin \beta_{V1} & -\cos \beta_{V1} & 0 \\ \sin \alpha_{V1} \cos \beta_{V1} & \sin \alpha_{V1} \sin \beta_{V1} & \cos \alpha_{V1} \end{bmatrix} \begin{bmatrix} -D_{VT1} \\ Y_{VT1} \\ 0 \end{bmatrix} \quad \text{(Eqn.2.168)}$$

$$\begin{bmatrix} L_{V1} \\ M_{V1} \\ N_{V1} \end{bmatrix} = \begin{bmatrix} Y_{V1} W_{VT1} - Z_{V1} B_{VT1} \\ Z_{V1} F_{VT1} - X_{V1} W_{VT1} \\ -Y_{V1} F_{VT1} + X_{V1} B_{VT1} \end{bmatrix} \quad \text{(Eqn.2.169)}$$

## CHAPTER THREE

### RESULTS

Four flight test is selected to validate the generic flight dynamics model. These flight tests are handling qualities step input and pulse input tests. After applying these tests, helicopter response is observed and flight test data and simulation data are compared. Step and pulse inputs are applied on four control channels which are roll, pitch, yaw and collective channels. Flight Test Configuration for All Transient Response Computations is given below:

Aircraft Inertia Values:

Ixx : 4659 slug-ft<sup>2</sup>

Iyy : 38512 slug-ft<sup>2</sup>

Izz : 36796 slug-ft<sup>2</sup>

Ixz : 1882 slug-ft<sup>2</sup>

Buttline CG location : 0 in.

Pitch bias actuator : disabled and centered

Flightpath stabilization : disabled

Stability augmentation system : disabled

Stabilator position : fixed to the trim value set by control system

Aircraft Configurations and Test Conditions for Transient Response Flight

Tests are as follows:

1. Test: 1 in left cyclic step input:

Gross Weight : 15770 lb

CG Stationline : 348.3 in

CG Waterline : 231.7 in

Pressure Altitude : 4514 ft

Airspeed : 73 knots

2. Test: 1 in aft cyclic pulse input:

Gross Weight :15510 lb  
CG Stationline : 352 in  
CG Waterline : 232 in  
Pressure Altitude : 5953 ft  
Airspeed : 70 knots

3. Test: 0.5 in up collective step input:

Gross Weight :15720 lb  
CG Stationline : 351.4 in  
CG Waterline : 231.8 in  
Pressure Altitude : 5515 ft  
Airspeed : 73 knots

4. Test: 1 in left pedal pulse input:

Gross Weight :16050 lb  
CG Stationline : 351.1 in  
CG Waterline : 232.4 in  
Pressure Altitude : 5953 ft  
Airspeed : 84 knots

Comparison results of real-time simulation and flight test data is given below:

### **3.1 First Test; 1 Inch Right Cyclic Step Input**

In this flight test, lateral cyclic step input is applied and the response of the helicopter is analyzed. The primary channel is the roll channel; therefore, while analyzing the responses, roll channel response is more important than other channels. Inputs are as below for this flight test:

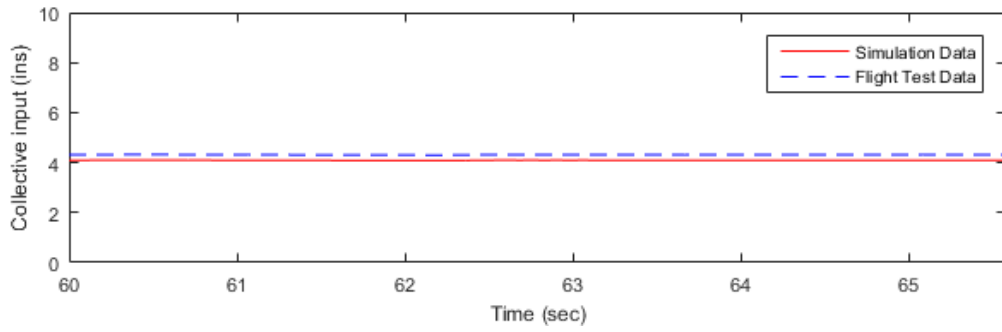


Figure 3.1: Collective input.

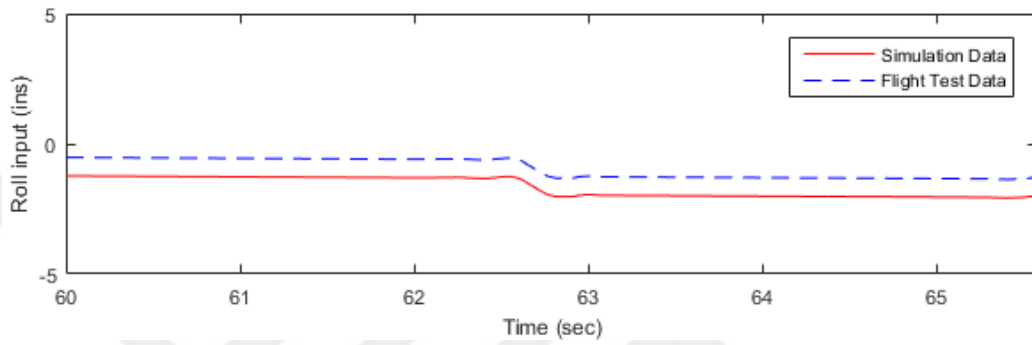


Figure 3.2: Roll input.

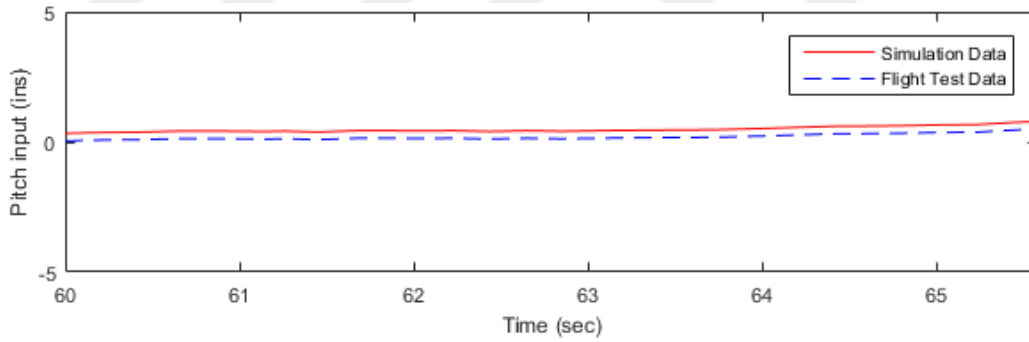


Figure 3.3: Pitch input.

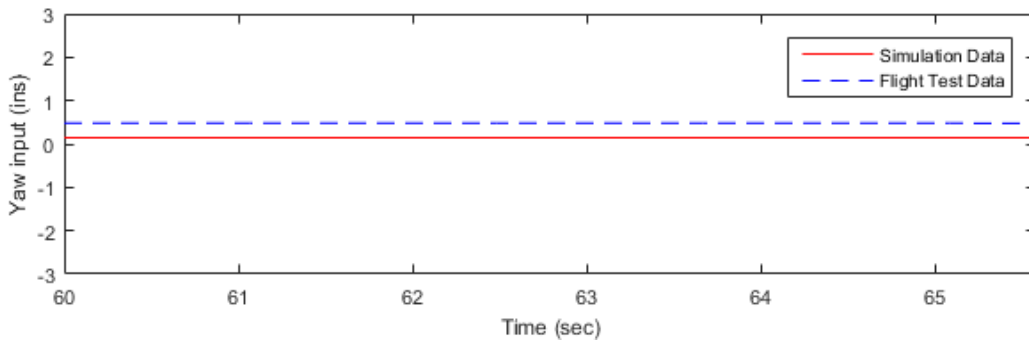


Figure 3.4: Yaw input.

Flight test and simulation attitude responses and comparisons are as below:

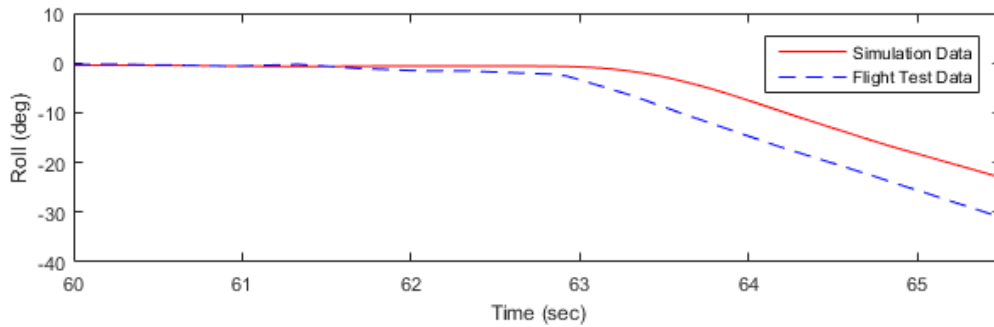


Figure 3.5: Roll attitude.

In roll channel, it can be seen the same trend for the two data but there is a lag in simulation data. Filters may be a reason for this lag.

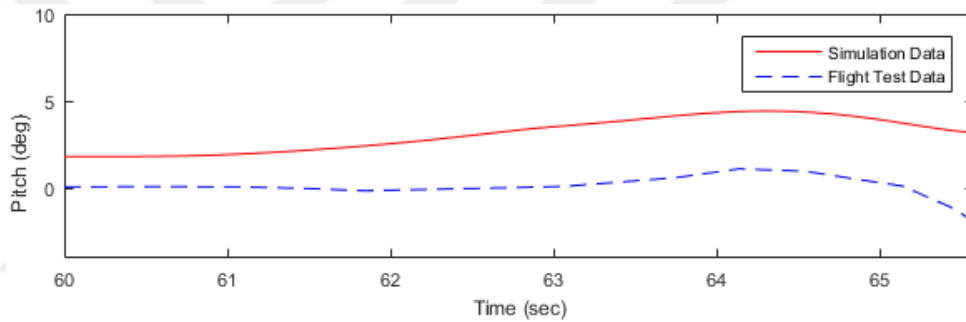


Figure 3.6: Pitch attitude.

In pitch channel, same trend can be seen and there is small difference between simulation and flight test data.

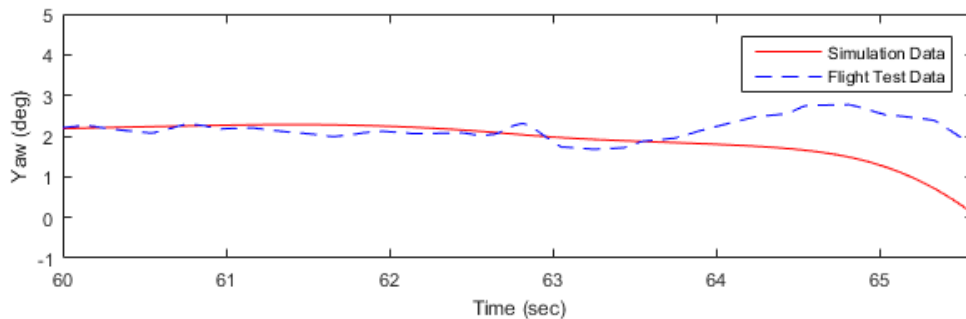
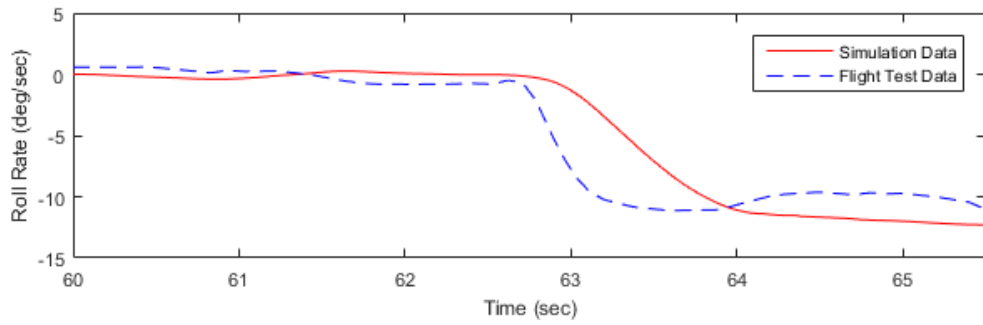


Figure 3.7: Yaw attitude.

In yaw channel, there is small disturbances in flight test. It is thought that environmental circumstances cause this small disturbances.

Flight test and simulation attitude rate responses and comparisons are given below:



**Figure 3.8:** Roll rate.

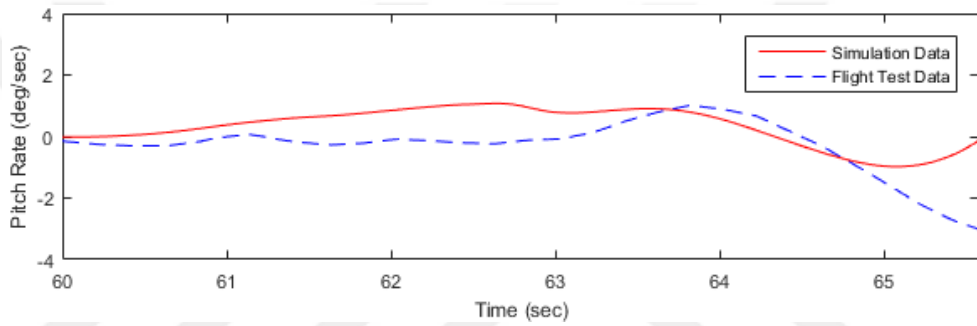


**Figure 3.9:** Pitch rate.

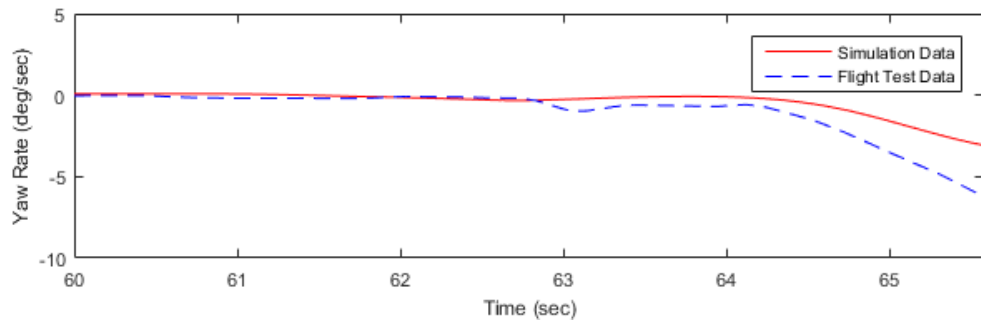


**Figure 3.10:** Yaw rate.

Vertical speed and indicated air speed comparison are presented below:

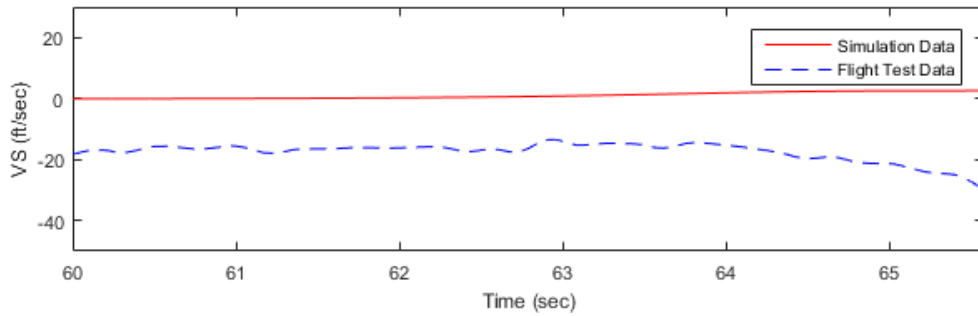


Figure 3.11: Vertical speed.

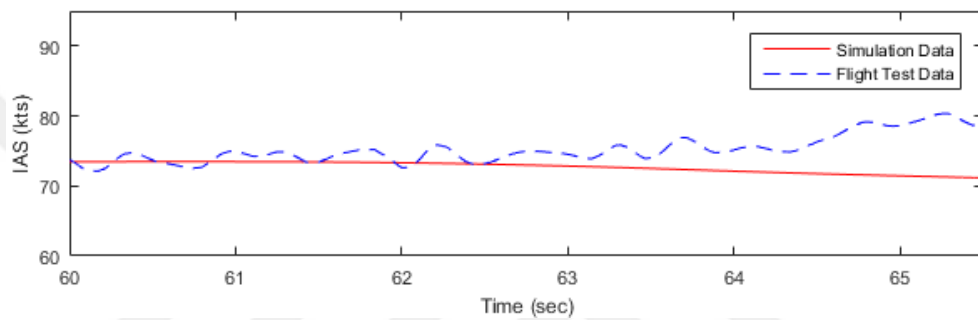


Figure 3.12: Indicated air speed.

### 3.2 Second Test; 1 Inch Aft Cyclic Pulse Input

In this flight test, longitudinal cyclic pulse input is applied and the response of the helicopter is analyzed. The primary channel is the pitch channel; therefore, while analyzing the responses, pitch channel response is more important than other channels. Inputs are as below for this flight test:

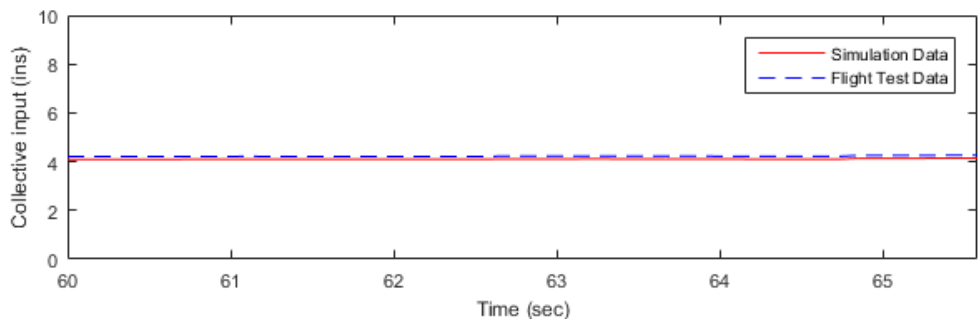


Figure 3.13: Collective input.

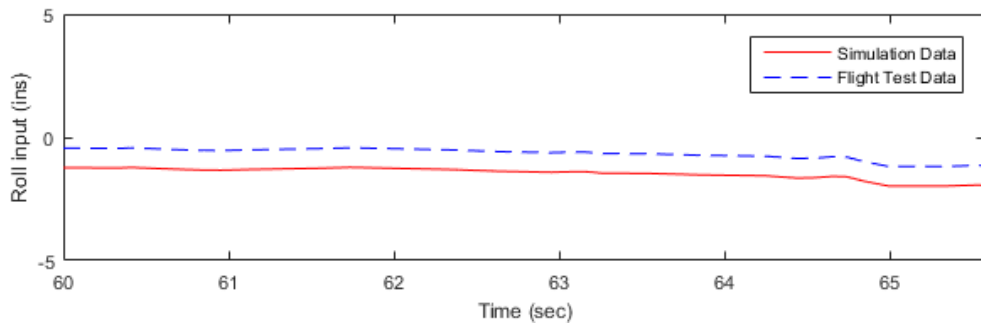


Figure 3.14: Roll input.

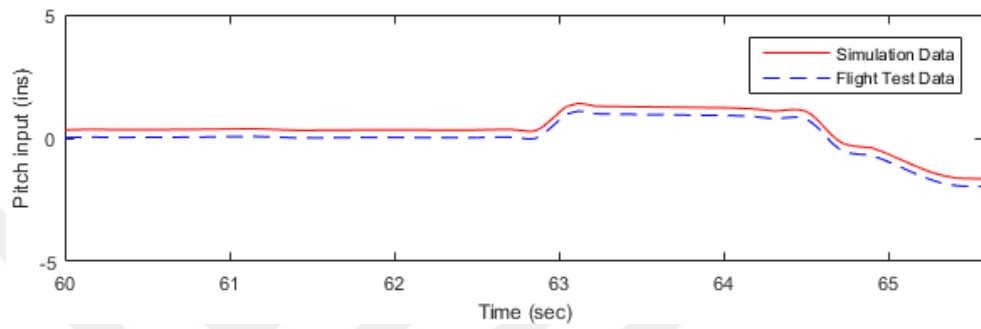


Figure 3.15: Pitch input.

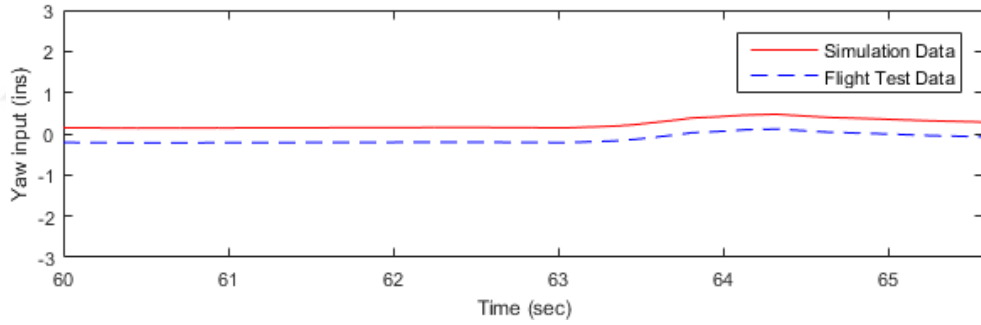


Figure 3.16: Yaw input.

Flight test and simulation attitude responses and comparisons are as below:

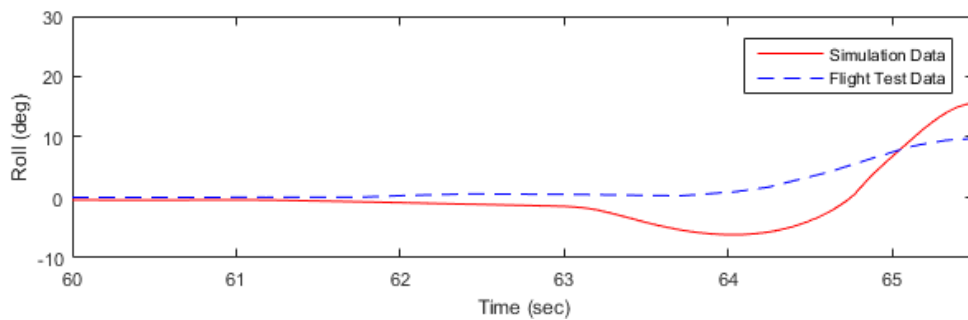
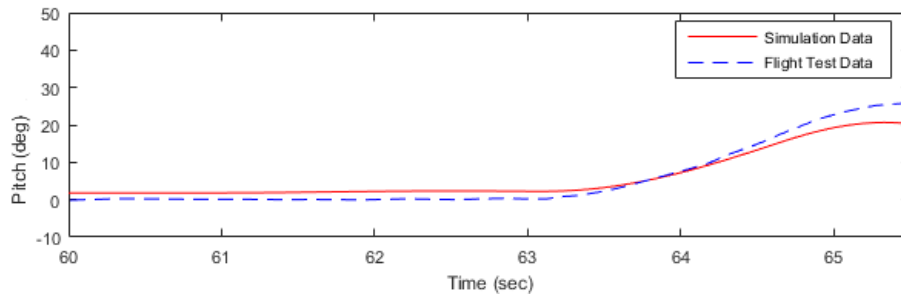


Figure 3.17: Roll attitude.



In roll channel, there is a small difference of behavior. But in this test roll channel is the secondary channel because input channel is pitch channel. Therefore, this small difference of behavior is acceptable. With fine-tuning this difference should be reduced.



**Figure 3.18:** Pitch attitude.

Pitch channel is the primary channel for this test. Simulation trend and values are very close to the flight test data.

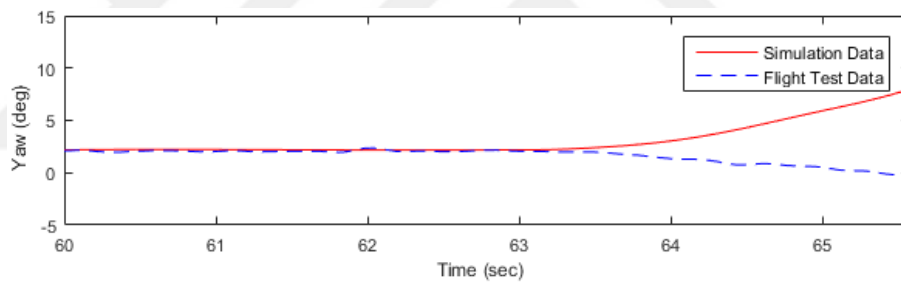


**Figure 3.19:** Yaw attitude.

In yaw channel, there is a small separation. This separation can be reduced with fine-tuning.

Flight test and simulation attitude rate responses and comparisons are given below:

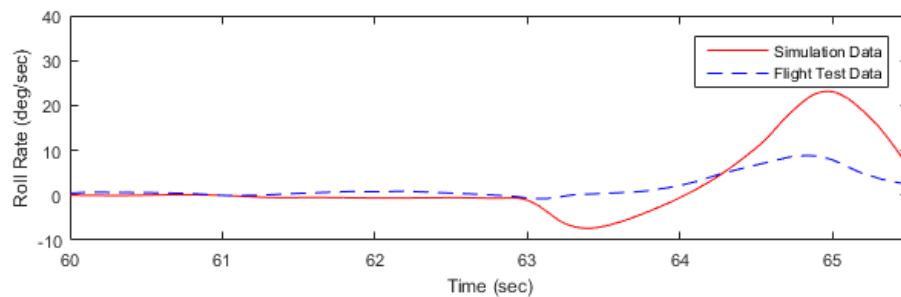


**Figure 3.20:** Roll rate.

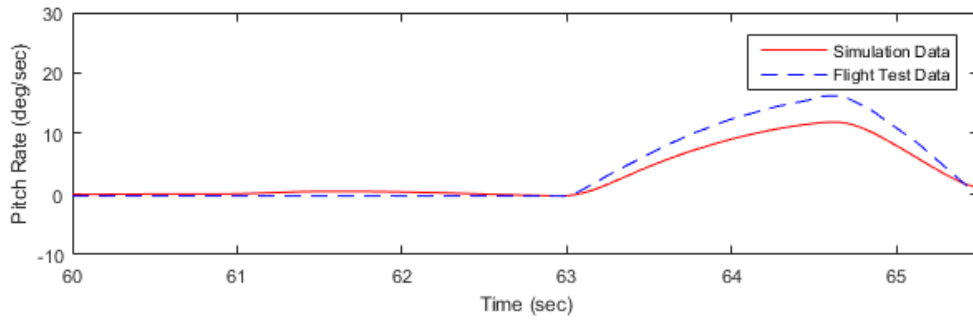


**Figure 3.21:** Pitch rate.

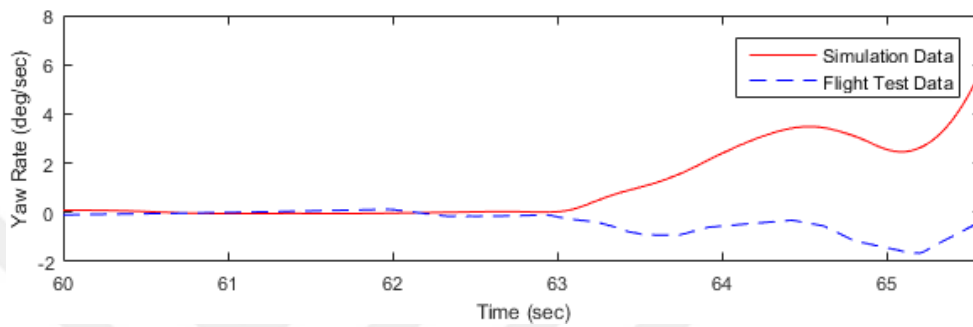


**Figure 3.22:** Yaw rate.

Vertical speed and indicated air speed comparison are presented below:

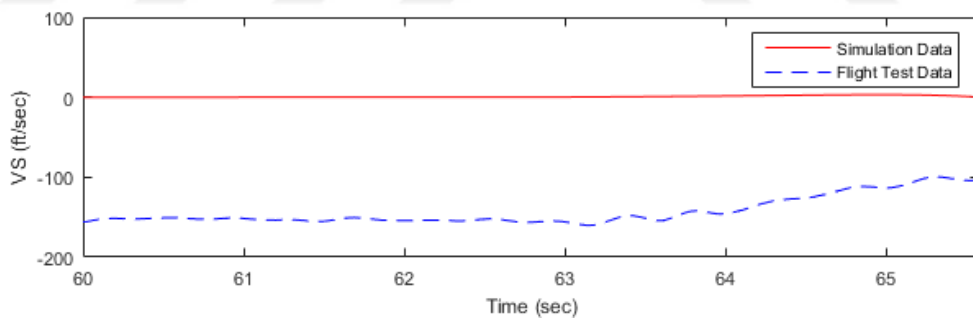


**Figure 3.23:** Vertical speed.

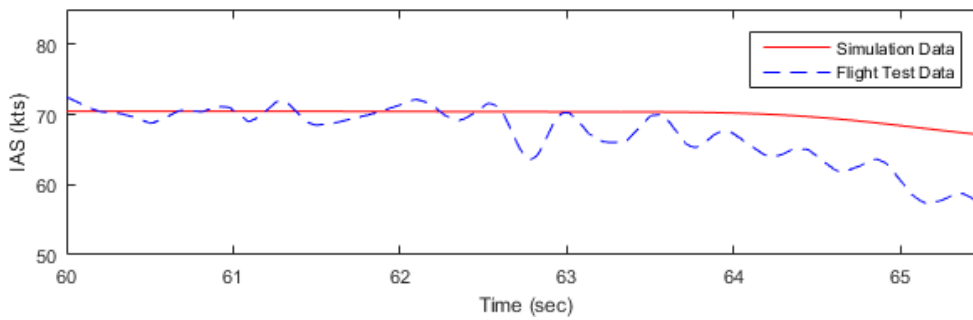


**Figure 3.24:** Indicated air speed.

### 3.3 Third Test; 0.5 Inch Collective Up Step Input

In this flight test, collective step input is applied and the response of the helicopter is analyzed. Inputs are as below for this flight test:

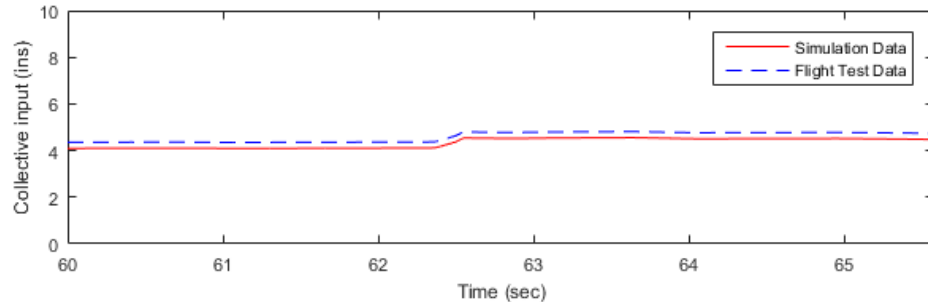


Figure 3.25: Collective input.

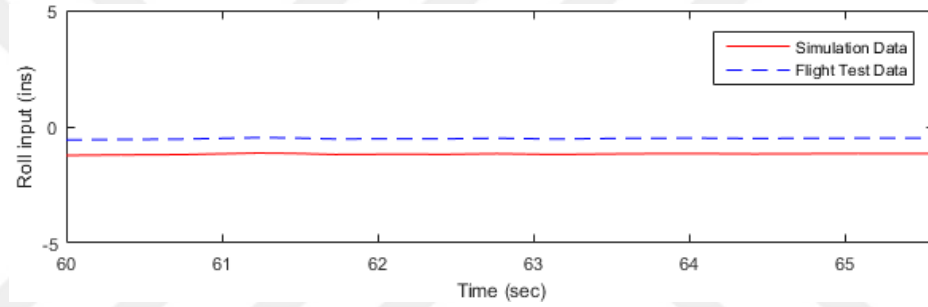


Figure 3.26: Roll input.

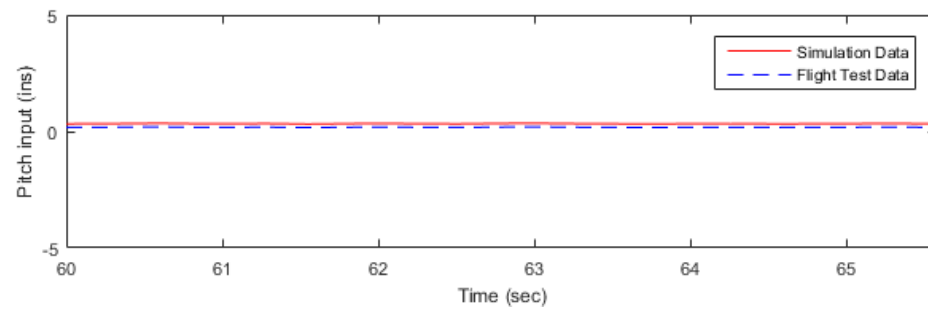


Figure 3.27: Pitch input.

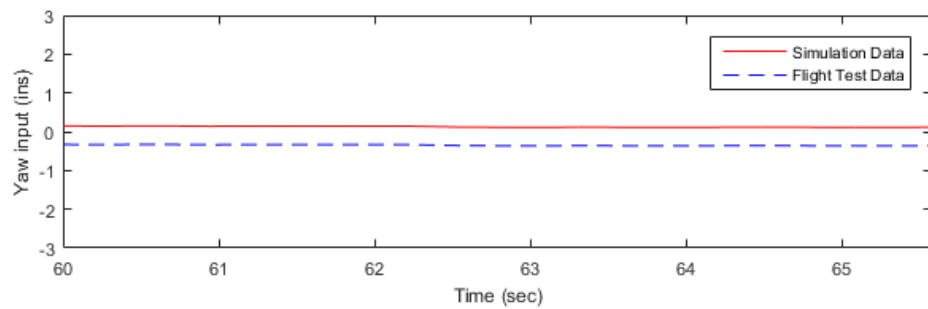
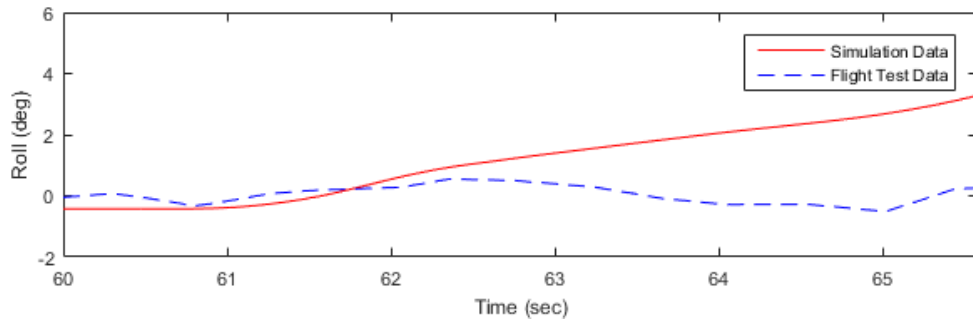


Figure 3.28: Yaw input.

Flight test and simulation attitude responses and comparisons are as below:



**Figure 3.29:** Roll attitude.

In roll channel, the simulation trend and values are so close to the flight test data.

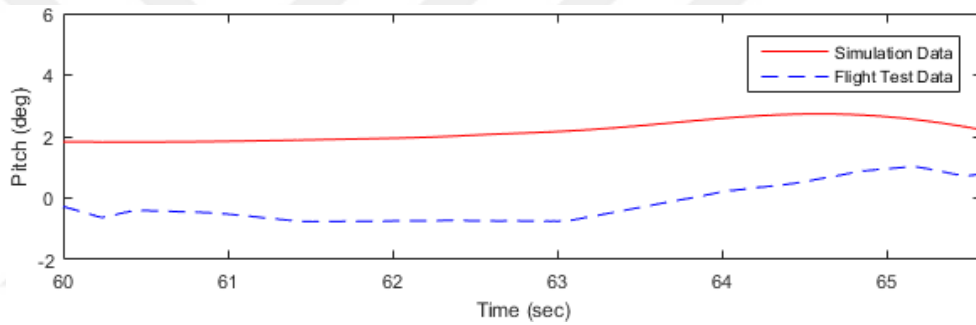


**Figure 3.30:** Pitch attitude.

In pitch channel, same trend can be seen and there is small difference between simulation and flight test data.

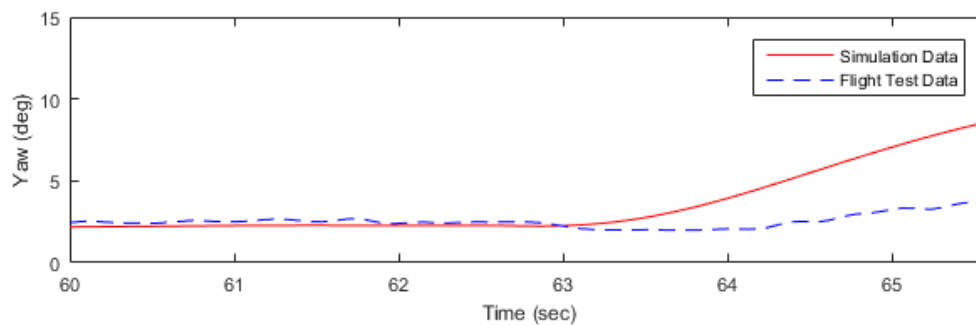


**Figure 3.31:** Yaw attitude.

In yaw channel, there is small disturbances in flight test most probably because of environmental circumstances. There is a small separation after step input. This separation can be reduce with fine-tuning.

Flight test and simulation attitude rate responses and comparisons are given below:

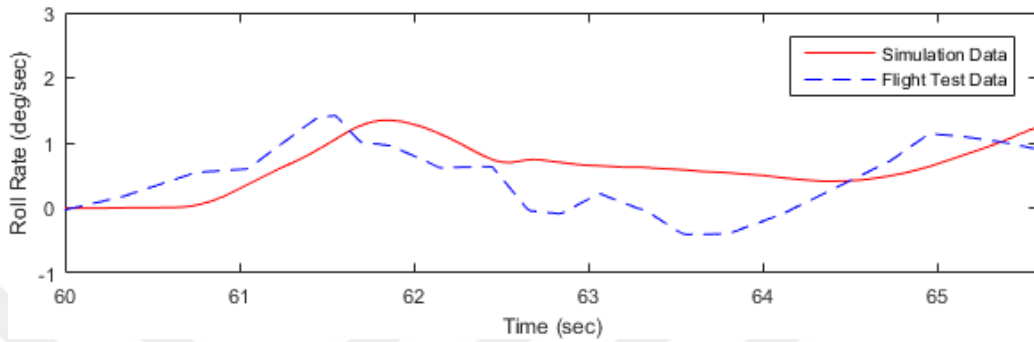


Figure 3.32: Roll rate.

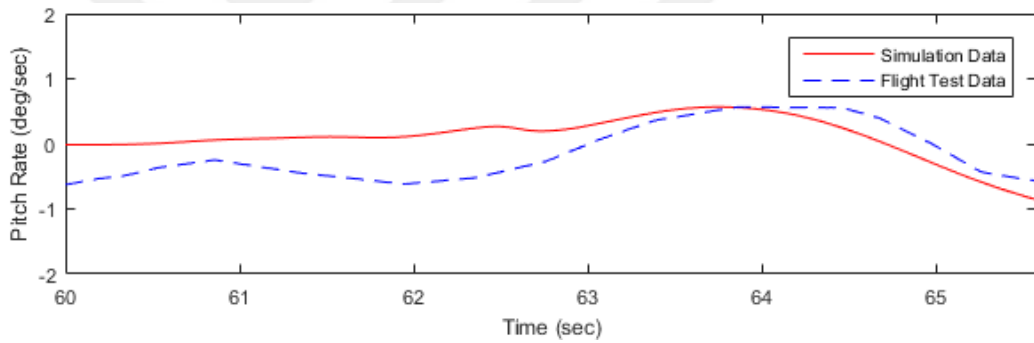


Figure 3.33: Pitch rate.

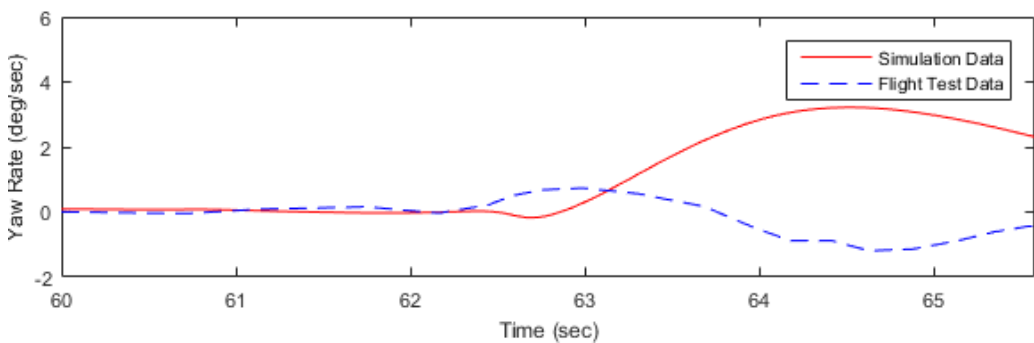


Figure 3.34: Yaw rate.

Vertical speed and indicated air speed comparison are presented below:

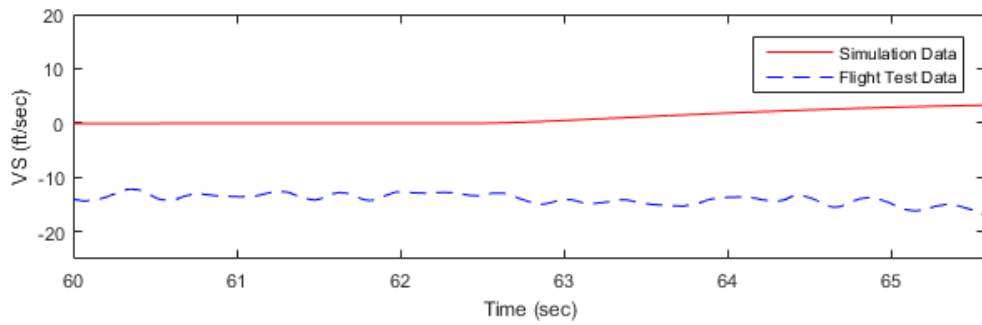


Figure 3.35: Vertical speed.

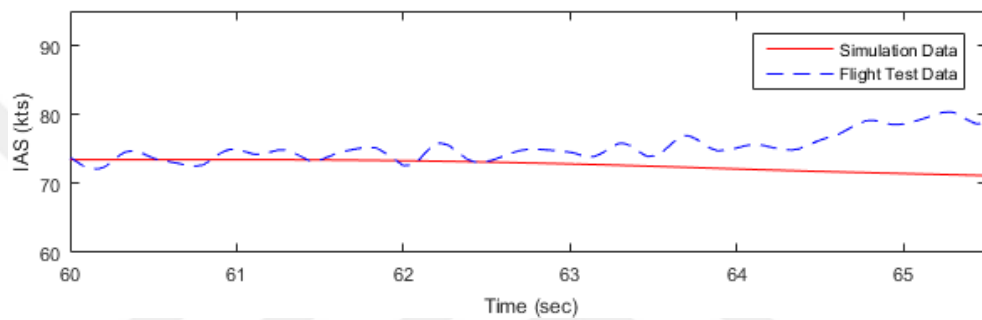


Figure 3.36: Indicated air speed.

### 3.4 Fourth Test; 1 Inch Left Pedal Pulse Input

In this flight test, pedal pulse input is applied and the response of the helicopter is analyzed. The primary channel is the yaw channel; therefore, while analyzing the responses, yaw channel response is more important than other channels. Inputs are as below for this flight test:

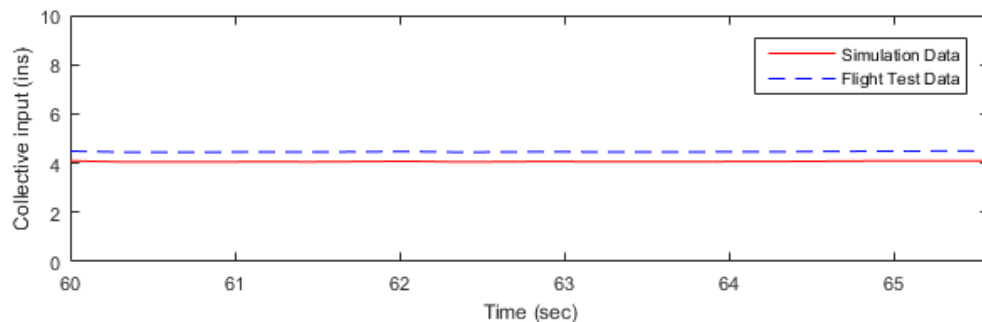


Figure 3.37: Collective input.

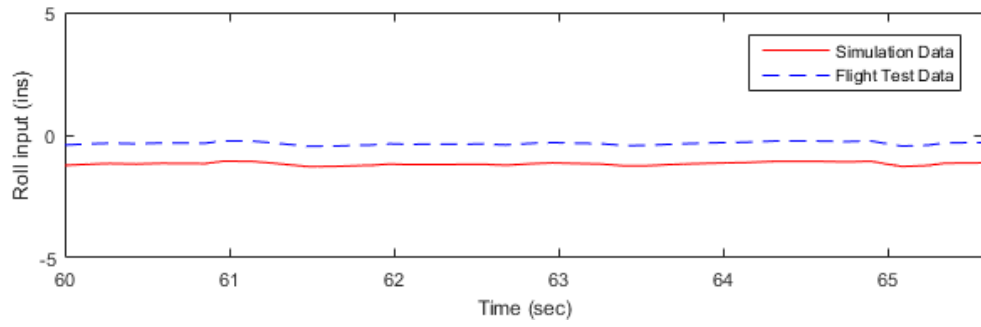


Figure 3.38: Roll input.

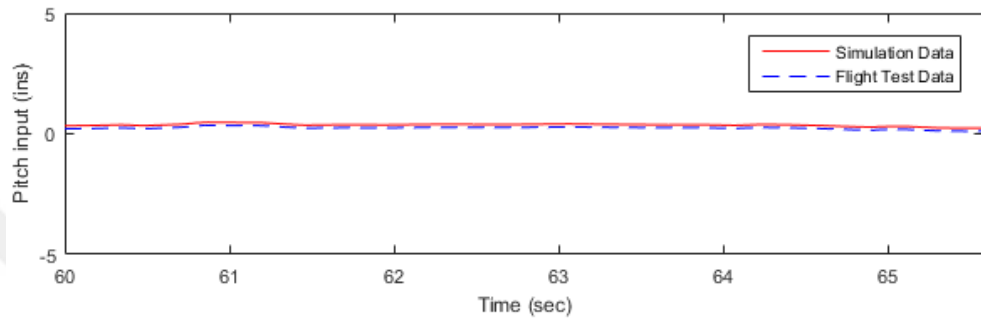


Figure 3.39: Pitch input.

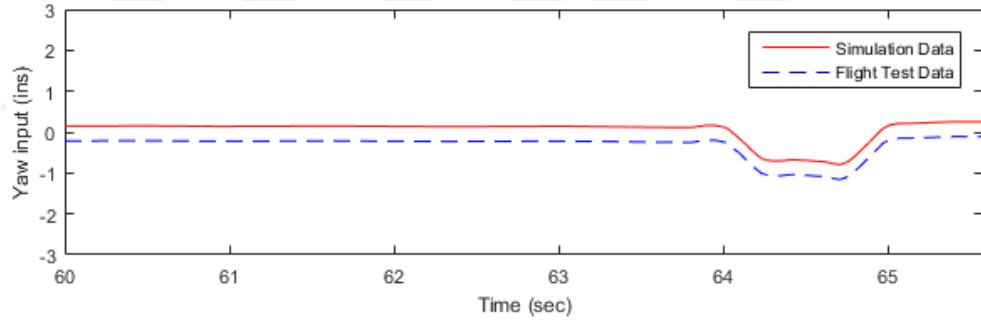


Figure 3.40: Yaw input.

Flight test and simulation attitude responses and comparisons are as below:

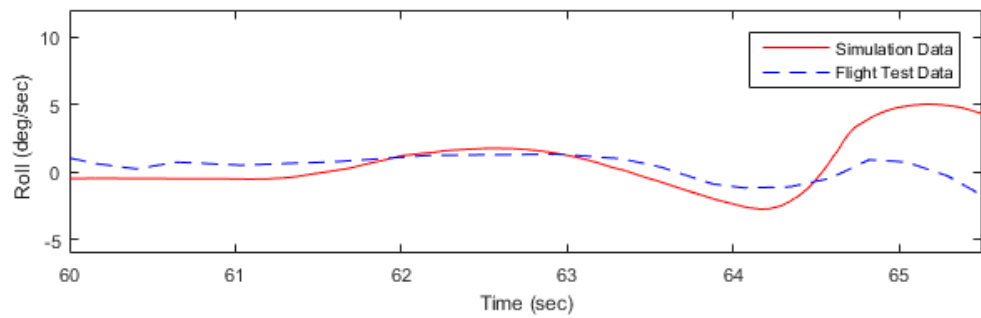
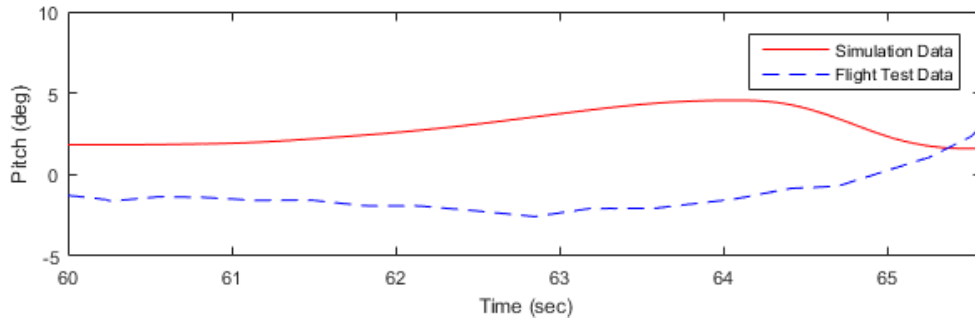


Figure 3.41: Roll attitude.

In roll channel, there is a small difference of behavior. But in this test roll channel is the secondary channel because input channel is yaw channel. Therefore, this small difference of behavior is acceptable. With fine-tuning this difference should be reduce.



**Figure 3.42:** Pitch attitude.

In pitch channel, there is a small difference of behavior. But in this test, roll channel is the secondary channel because input channel is yaw channel. With fine-tuning small differences between simulation and flight test data can reduce.

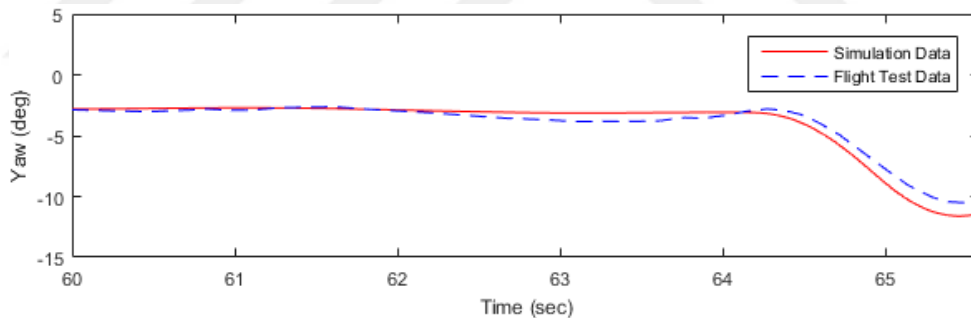


**Figure 3.43:** Yaw attitude.

Yaw channel is the primary channel for this test. Simulation trend and values are very close to the flight test data.



Flight test and simulation attitude rate responses and comparisons are given below:

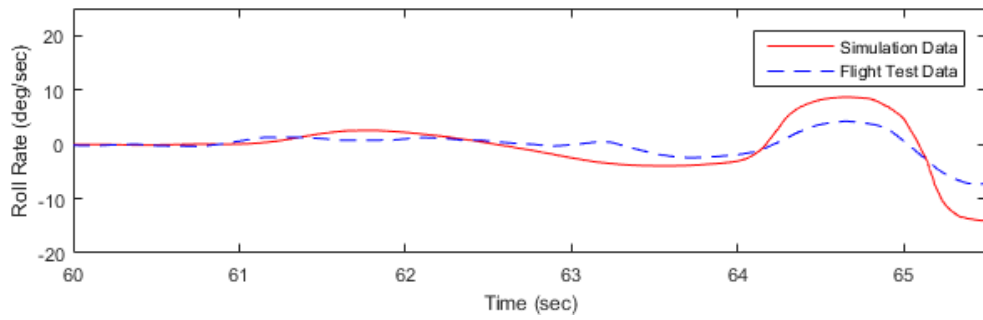


Figure 3.44: Roll rate.

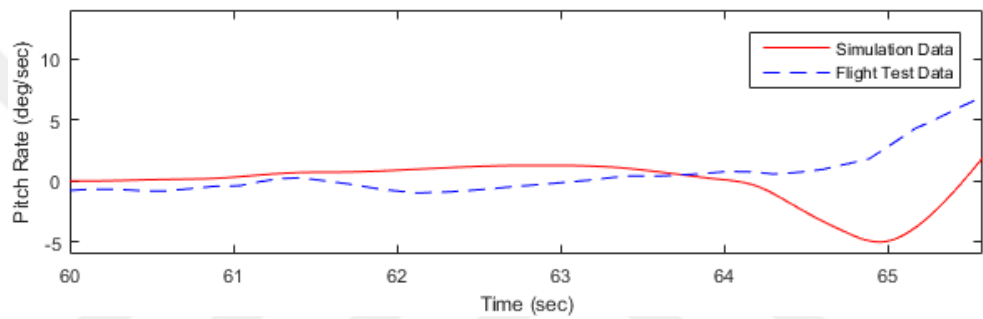


Figure 3.45: Pitch rate.

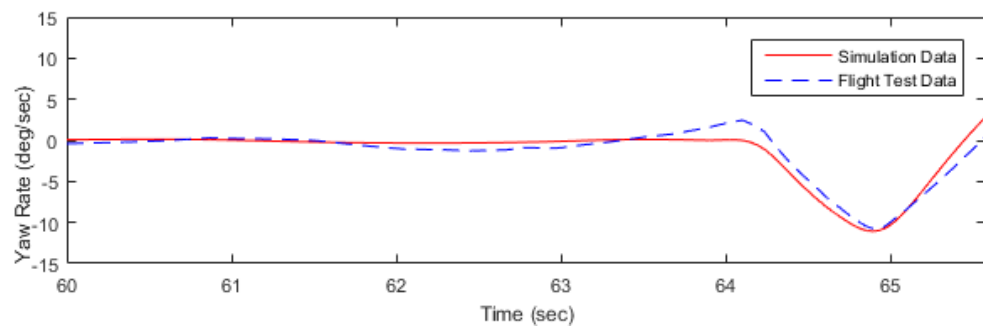
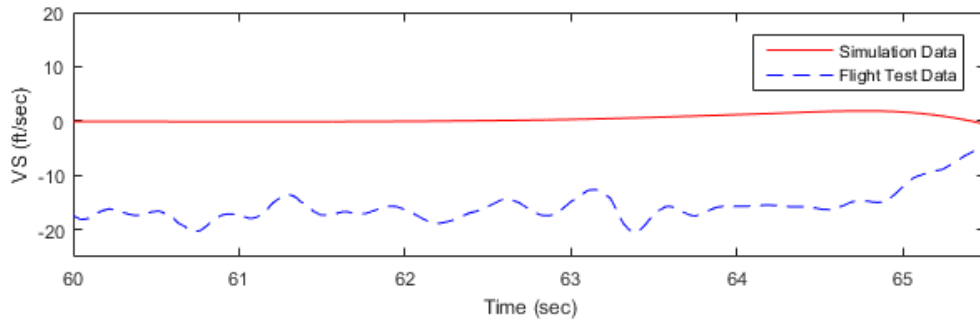
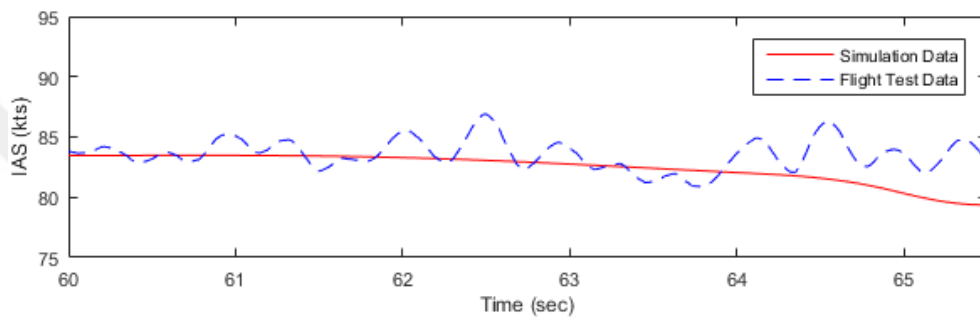


Figure 3.46: Yaw rate.

Vertical speed and indicated air speed comparison are presented below:



**Figure 3.47:** Vertical speed.



**Figure 3.48:** Indicated air speed.

For all tests, from the input data comparison, it can be claimed that simulation controls trim position differences between flight test control positions are below 10% of the total travel range of the control channels. Longitudinal cyclic and collective trim positions are very close to flight test longitudinal cyclic and collective trim positions. Lateral cyclic and pedal trim positions are also close to flight test control trim positions; nevertheless, the difference can be smaller with fine tuning studies. From the attitude data comparison, simulation roll attitude trim values are so close to flight test roll attitude trim values. Approximately 2 degrees difference is observed at pitch attitude trim values between simulation and flight test data.

## CHAPTER FOUR

### CONCLUSION

Four tests are applied to validate the helicopter dynamics mathematical model which is explained in this thesis study. These four tests are handling quality tests with step and pulse inputs. Four different control channel inputs are handled in four different tests. Each test, input is given at only one control channel. It is seen at results graphs that simulation controls trim position differences with respect to flight test control positions are below 10% of the total travel range of the control channels. Longitudinal cyclic trim position is very close to flight test longitudinal cyclic trim positions. Lateral cyclic and pedal trim positions are also close to flight test control trim positions; nevertheless, the difference can be smaller with fine tuning studies. From all comparisons of simulation and flight test data, simulation roll attitude trim values are so close to flight test roll attitude trim values. There is approximately 2 degrees difference at pitch attitude trim values between simulation and flight test data which is very small difference. According to QTG, primary parameters to be analysed are attitude and attitude rate of axis of input applied. At first test, input is applied at the roll channel. In this test, roll attitude and roll rate Show the same trend. The only difference is that there is a lag at simulation data with respect to flight test data. For the second test, longitudinal cyclic pulse input is applied. Pitch attitude and pitch rate Show the same trend and close values. In roll channel, there is a small difference of behavior. But in this test roll channel is the secondary channel because input channel is pitch channel. Therefore, this small difference of behavior is acceptable. With fine-tuning this difference should be reduced. Collective step input is applied at the third test. Roll and pitch attitude and rates have same behaviour and close values. At the fourth test, pulse input is given to the pedals. In this test, yaw attitude and yaw rate behaviour and values are very close to the flight test data.

## REFERENCES

- [1] F. J. Bailey, J., "A Simplified Theoretical Method of Determining the Characteristics of a Lifting Rotor in Forward Flight," Naca report 716, NACA, 1941.
- [2] Chen, R. T. N., "A Simplified Rotor System Mathematical Model for Piloted Flight Dynamics Simulation," Nasa-tm-78575, NASA, 1979.
- [3] Chen, R. T. N., "Effects of Primary Rotor Parameters on Flapping Dynamics," Nasa-tp-1431, NASA, 1980.
- [4] P. D. Talbot, B. E. Tinling, W. A. D. and Chen, R. T. N., "Mathematical Model of a Single Main Rotor Helicopter for Piloted Simulations," Nasa-tm-84281, NASA, 1982.
- [5] Howlett, J. J., "UH-60A Black Hawk Engineering Simulation Program: Volume I - Mathematical Model," Nasa-cr-166309, NASA, 1981.
- [6] Hilbert, K. B., "A Mathematical Model of the UH-60 Helicopter," Nasa-tm-85890, NASA, 1984.
- [7] Kaplita, T. T., "UH-60 Black Hawk Engineering Simulation Model Validation and Proposed Modifications," Nasa-cr-177360, NASA, 1985.
- [8] Hefley, R. K. and Mnich, M. A., "Minimum-Complexity Helicopter Simulation Math Model," Nasa-cr-177476, NASA, 1988.
- [9] Mark E. Dreier, "Introduction to Helicopter and Tiltrotor Flight Simulation," AIAA Education Series, 2007.
- [10] K. Braman, S. Ramachadran, "Helicopter Simulation Techniques For Full Mission Flight Simulation," I/ITSEC, 1986.
- [11] J. Gordon Leishman, "Principles of Helicopter Aerodynamics," Cambridge Aerospace Series, Second Edition, 2006.

- [12] Wayne Johnson, "Rotorcraft Aeromechanics," Cambridge University Press, 2013.
- [13] John Seddon and Simon Newman, "Basic Helicopter Aerodynamics," A John Wiley & Sons, Ltd., Publication, Third Edition, 2011.
- [14] Suwan Park, Nakhoon Baek, Kwan Woo- Ryu, "A Dynamics Model of Rotor Blades for Real-time Helicopter Simulation", International Journal of Multimedia and Ubiquitous Engineering Vol. 7, No. 2, April, 2012.
- [15] I.C. Cheeseman and W. E. Bennett, "The Effect of the Ground on a Helicopter Rotor in Forward Flight", 1957.



## APPENDIX

<b>1. Appendix -A: Symbol Definitions of Equations.....</b>	<b>51</b>
---	-----------



## Appendix-A: Symbol Definitions of Equations

**Table A.1:** Notations for the main rotor module.

Symbols	Units	Description
(IB)	INDEX	Indicating 1...NBS blades simulated
(IS)	INDEX	Indicating 1...NSS segments/blade simulated
(I)	INDEX	Indicating 1...(NBS-1 )NSS blade segments
$\xi$	FT	Blade hinge offset from center of rotation
$\xi'$	FT	Spar length exposed
R	FT	Rotor radius
$\Omega_T$	RADS/SEC	Rotor nominal input rotational speed
e	-	Normalized offset
e'	-	Normalized spar length
$y_{2IS}$	-	Distance from hinge to segment midpoint
$C_{yIS}$	FT	Segment chord
$C_T$	FT	Blade top chord
$C_R$	FT	Blade root chord
$S_{yIS}$	FT <sup>2</sup>	Blade segment area
b	-	Number of rotor blades
$\dot{U}_{Body}$	FT/SEC <sup>2</sup>	Accel . along X-axis
$\dot{V}_{Body}$	FT/SEC <sup>2</sup>	Accel. along Y-axis
$\dot{W}_{Body}$	FT/SEC <sup>2</sup>	Accel . along Z-axis
$\dot{p}$	RADS/SEC <sup>2</sup>	Angular accel about X-axis
$\dot{q}$	RADS/SEC <sup>2</sup>	Angular accel about Y-axis
$\dot{r}$	RADS/SEC <sup>2</sup>	Angular accel about Z-axis
$U_{Body}$	FT/SEC	Vel. along X-axis
$V_{Body}$	FT/SEC	Vel. along Y-axis
$w_{Body}$	FT/SEC	Vel. along Z-axis
p	RADS/SEC	Angular rate about X-axis
q	RADS/SEC	Angular rate about Y-axis

**Table A.1 (Continue):** Notations for the main rotor module.

$r$	RADS/SEC	Angular rate about Z-axis
$X_H$	FT	Longitudinal rotor arm
$Y_H$	FT	Lateral rotor arm
$Z_H$	FT	Vertical rotor arm
$g_x$	FT/SEC <sup>2</sup>	Gravity vectors
$g_y$	FT/SEC <sup>2</sup>	
$g_z$	FT/SEC <sup>2</sup>	
$\mu_{XH}$	-	hub velocities - normalized
$\mu_{YH}$	-	
$\mu_{ZH}$	-	
$\mu_{XS}$	-	shaft velocities - normalized
$\mu_{YS}$	-	
$\mu_{ZS}$	-	
$p_s$	RADS/SEC	Shaft angular rates
$q_s$	RADS/SEC	
$r_s$	RADS/SEC	
$\dot{p}_s$	RADS/SEC <sup>2</sup>	Shaft angular acceleration
$\dot{q}_s$	RADS/SEC <sup>2</sup>	
$\dot{r}_s$	RADS/SEC <sup>2</sup>	
$\dot{U}_{Hub}$	FT/SEC <sup>2</sup>	Hub accelerations
$\dot{V}_{Hub}$	FT/SEC <sup>2</sup>	
$\dot{W}_{Hub}$	FT/SEC <sup>2</sup>	
$\dot{V}_{XS}$	FT/SEC <sup>2</sup>	Shaft accelerations
$\dot{V}_{YS}$	FT/SEC <sup>2</sup>	
$\dot{V}_{ZS}$	FT/SEC <sup>2</sup>	
$\Omega$	RADS/SEC	Rotor shaft speed
$\Omega_T$	RADS/SEC	Rotor shaft datum speed
$\psi$	DEG	Rotor azimuth position
$\beta$	RADS	Flapping angle
$\dot{\beta}$	RADS/SEC	Flapping rate
$\ddot{\beta}$	RADS/SEC <sup>2</sup>	Flapping acceleration
$\delta$	RADS	Lagging angle
$\dot{\delta}$	RADS/SEC	Lagging rate
$\ddot{\delta}$	RADS/SEC <sup>2</sup>	Lagging acceleration



**Table A.1 (Continue):** Notations for the main rotor module.

$\mu_{TOT}$	-	Total velocity component at the rotor
$K_{1X}$	-	Longitudinal Glauert inflow factor
$K_{1Y}$	-	Lateral Glauert inflow factor
$T_{HA}$	LB	Aerodynamic component of thrust
$M_{HA}$	FT LB	Aerodynamic component of pitching moment
$L_{HA}$	FT LB	Aerodynamic component of rolling moment
$\rho$	SLUGS/FT <sup>3</sup>	Air density
$C_{TA}$	-	Thrust coefficient
$C_{MHA}$	-	Pitching moment coefficient
$C_{LHA}$	-	Rolling moment coefficient
$D_{W0}$	1/RADS	Uniform component of downwash at the rotor disk
$D_{WC}$	1/RADS	Cosine component of downwash
$D_{WS}$	1/RADS	Sine component of downwash
$U_{PDI}$	1/RADS	Total components of downwash in blade span axes
$\lambda$	1/RADS	Total normal rotor inflow velocity
$U_{PAIB}$	1/RADS	Blade segment total velocity components in blade span axes
$U_{PBIB}$	1/RADS	
$U_{PI}$	1/RADS	
$U_{TAIB}$	1/RADS	
$U_{TBIB}$	1/RADS	
$U_{TI}$	1/RADS	
$U_{YI}$	1/RADS	Total flow component at the blade segment
$M$	-	Blade segment Mach Number
$a$	FT/SEC	Speed of sound
$b_s$	-	Number of blades simulated
$NSS$	-	Number of segments simulated
$F_{PI}$	LB	Segment aero forces
$F_{TI}$	LB	
$F_{PB}$	LB	Blade aero forces - blade span axis
$F_{TB}$	LB	
$F_{XA}$	LB	Blade aero forces-shaft rotating axis
$F_{YA}$	LB	
$F_{ZA}$	LB	

**Table A.1 (Continue):** Notations for the main rotor module.

$M_{FAB}$	FT LB	Aero moments about hinge-blade span axis
$M_{LAB}$	FT LB	
$I_b$	SLUGS FT <sup>2</sup>	Inertia of blade about the hinge
$H_H$	LB	Total force component outputs from the rotor in shaft axes at the hub
$J_H$	LB	
$T_H$	LB	
$L_H$	FT LB	Total moment component outputs from the rotor in shaft axes at the hub
$M_H$	FT LB	
$Q_H$	FT LB	
$X_{MR}$	LB	Rotor forces and moments in body axes at the fuselage c.g.
$Y_{MR}$	LB	
$Z_{MR}$	LB	
$L_{MR}$	FT LB	
$M_{MR}$	FT LB	
$N_{MR}$	FT LB	

**Table A.2:** Notations for the fuselage module.

Symbols	Units	Description
$V_{XWF}$	FT/SEC	Total velocity components at the fuselage center of gravity
$V_{YWF}$	FT/SEC	
$V_{ZWF}$	FT/SEC	
$V_{XIWF}$	FT/SEC	Rotor wash interference on the fuselage.
$V_{YIWF}$	FT/SEC	
$V_{ZIWF}$	FT/SEC	
QWF	LB/FT <sup>2</sup>	Dynamic pressure at the body
$\alpha_{WF}$	DEG	Body axis angle of attack
$\beta_{WF}$	DEG	Sideslip angle
DQFTOT	FT <sup>2</sup>	Total components of aerodynamic coefficients at the wind tunnel mounting point in wind axes
YQFTOT	FT <sup>2</sup>	
LQFTOT	FT <sup>2</sup>	
RQFTOT	FT <sup>3</sup>	
MQFTOT	FT <sup>3</sup>	
NQFTOT	FT <sup>3</sup>	
FS <sub>CGB</sub>	INS	Fuselage station for the fuselage C.G.
WL <sub>CGB</sub>	INS	Waterline station for the fuselage C.G.
FS <sub>WF</sub>	INS	Fuselage station for tunnel mounting point
WL <sub>WF</sub>	INS	Water line station for tunnel mounting point
F <sub>WT</sub>	FT	Fuselage longitudinal mounting point arm
W <sub>WT</sub>	FT	Fuselage vertical mounting point arm
B <sub>WT</sub>	FT	Fuselage lateral mounting point arm
D <sub>FUS</sub>	LB	Fuselage aerodynamic component loads in wind axis
Y <sub>FUS</sub>	LB	
L <sub>FUS</sub>	LB	
R <sub>FUS</sub>	FT LB	
M <sub>FUS</sub>	FT LB	
N <sub>FUS</sub>	FT LB	
X <sub>WF</sub>	LB	Fuselage aerodynamic component loads in body axes at the C.G.
Y <sub>WF</sub>	LB	
Z <sub>WF</sub>	LB	
L <sub>WF</sub>	FT LB	
M <sub>WF</sub>	FT LB	
N <sub>WF</sub>	FT LB	
V <sub>XgWF</sub>	FT/SEC	Guset velocities at the fuselage
V <sub>YgWF</sub>	FT/SEC	
V <sub>ZgWF</sub>	FT/SEC	

**Table A.3:** Notations for the horizontal and vertical tail module.

Symbols	Units	Description
$FS_{H1}$	FT	Fuselage station for horizontal tail C.P.
$FS_{CGB}$	FT	Fuselage station for CG
$F_{HT1}$	FT	Fuselage longitudinal moment arm
$WL_{H1}$	FT	Waterline station for horizontal tail C.P.
$WL_{CGB}$	FT	Waterline station for CG
$W_{HT1}$	FT	Fuselage vertical moment arm
$BL_{H1}$	FT	Buttline station for horizontal tail C.P.
$BL_{CGB}$	FT	Buttline station for CG
$B_{HT1}$	FT	Fuselage lateral moment arm
$V_{XMRH1}$	FT/SEC	Rotor interference velocity at the horizontal tail
$V_{YMRH1}$	FT/SEC	
$V_{ZMRH1}$	FT/SEC	
$K_{QH1}$	-	Square root of dynamic pressure ratio
$V_{Xb}$	FT/SEC	Fuselage X axis velocity
$V_{Yb}$	FT/SEC	Fuselage Y axis velocity
$V_{Zb}$	FT/SEC	Fuselage Z axis velocity
$V_{ZWFH1}$	FT/SEC	Fuse/Tail downwash velocity
$V_{XIH1}$	FT/SEC	Horizontal tail total interference velocity
$V_{YIH1}$	FT/SEC	
$V_{ZIH1}$	FT/SEC	
$p$	RADS/SEC	Body axes angular rates
$q$	RADS/SEC	
$r$	RADS/SEC	
$V_{XH1}$	FT/SEC	Total velocity at the horizontal tail
$V_{YH1}$	FT/SEC	
$V_{ZH1}$	FT/SEC	
$V_{XgH1}$	FT/SEC	Gust velocity at the horizontal tail
$V_{YgH1}$	FT/SEC	
$V_{ZgH1}$	FT/SEC	
$\rho$	SLUG/FT	Air density
$Q_{H1}$	LB/FT <sup>2</sup>	Dynamic pressure at the horizontal tail
$\alpha_{HH1}$	DEG	Total tail angle of attack
$\beta_{H1}$	DEG	Sideslip angle
$V_{XMRV1}$	FT/SEC	Rotor interference velocities
$V_{YMRV1}$	FT/SEC	
$V_{ZMRV1}$	FT/SEC	
$V_{YWFV1}$	FT/SEC	Fuselage sidewash velocity
$V_{XV1}$	FT/SEC	Total velocity at the vertical tail
$V_{YV1}$	FT/SEC	

**Table A.3 (Continue):** Notations for the horizontal and vertical tail module.

$V_{ZV1}$	FT/SEC	
$V_{XgV1}$	FT/SEC	Gust velocity at the vertical tail
$V_{YgV1}$	FT/SEC	
$V_{ZgV1}$	FT/SEC	
$V_{XIV1}$	FT/SEC	
$V_{YIV1}$	FT/SEC	
$V_{ZIV1}$	FT/SEC	
$Q_{V1}$	LB/FT <sup>2</sup>	Dynamic pressure at the vertical tail
$\alpha_{V1}$	DEG	Angle of attack
$\beta_{V1}$	DEG	Sideslip
$C_{LH1}$	-	Horizontal tail coefficient of lift
$C_{DH1}$	-	Horizontal tail coefficient of drag
$X_{H1}$	LB	Horizontal tail forces and moments
$Y_{H1}$	LB	
$Z_{H1}$	LB	
$L_{H1}$	FT LB	
$M_{H1}$	FT LB	
$N_{H1}$	FT LB	
$FS_{VT1}$	FT	Fuselage station for the vertical tail C.P.
$F_{VT1}$	FT	Fuselage longitudinal moment arm
$WL_{VT1}$	FT	Waterline Station for the vertical tail C.P.
$BL_{VT1}$	FT	Buttline Station for the vertical tail C.P.
$W_{VT1}$	FT	Fuselage vertical moment arm
$B_{VT1}$	FT	Fuselage lateral moment arm
$Q_{V1}$	-	Dynamic pressure ratio
$K_{QV1}$	-	SQRT (dynamic pressure ratio)
$C_{LV1}$	-	Vertical tail coefficient of lift
$C_{DV1}$	-	Vertical tail coefficient of drag
$X_{V1}$	LB	Vertical tail forces and moments
$Y_{V1}$	LB	
$Z_{V1}$	LB	
$L_{V1}$	FT LB	
$M_{V1}$	FT LB	
$N_{V1}$	FT LB	

**Table A.4:** Notations for the tail rotor module.

Symbols	Units	Description
$FS_{TR}$	FT	Fuselage station for tail rotor
$FS_{CGB}$	FT	Fuselage station for CG
$F_{TR}$	FT	Tail rotor longitudinal arm
$WL_{TR}$	FT	Waterline station for tail rotor
$WL_{CGB}$	FT	Waterline station for CG
$W_{TR}$	FT	Tail rotor vertical arm
$BL_{TR}$	FT	Buttline station for tail rotor
$BL_{CGB}$	FT	Buttline station for the CG
$B_{TR}$	FT	Tail rotor lateral arm
$D_{WSHTR}$	-	Uniform downwash at the main rotor
$V_{XMRTR}$	FT/SEC	Main rotor wash at the tail rotor
$V_{YMRTR}$	FT/SEC	
$V_{ZMRTR}$	FT/SEC	
$K_{QTR}$	-	Square root of dynamic pressure ratio
$V_{Xb}$	FT/SEC	Body axes velocities
$V_{Yb}$	FT/SEC	
$V_{Zb}$	FT/SEC	
$V_{YWFTR}$	FT/SEC	Fuselage sidewash velocity
$V_{ZWFTR}$	FT/SEC	Fuselage downwash velocity
$V_{XITR}$	FT/SEC	Total interference velocities at the tail rotor
$V_{YITR}$	FT/SEC	
$V_{ZITR}$	FT/SEC	
$V_{XgTR}$	FT/SEC	Body axes gust velocities
$V_{YgTR}$	FT/SEC	
$V_{ZgTR}$	FT/SEC	
$p$	RADS/SEC	Body axes angular rates
$q$	RADS/SEC	
$r$	RADS/SEC	
$V_{XTRB}$	FT/SEC	Total velocities at the tail rotor in body axes
$V_{YTRB}$	FT/SEC	
$V_{ZTRB}$	FT/SEC	

**Table A.4 (Continue):** Notations for the tail rotor module.

$V_{XTR}$	FT/SEC	Total velocities at the tail rotor in shaft axes
$V_{YTR}$	FT/SEC	
$V_{ZTR}$	FT/SEC	
$\Gamma_{TR}$	DEG	Tail rotor cant angle
$\Omega_{TR}$	RADS/SEC	Tail rotor trim speed
$R_{TR}$	FT	Tail rotor radius
$\mu_{XTR}$	-	Shaft axes velocities normalized by rotor tip speed
$\mu_{YTR}$	-	
$\mu_{ZTR}$	-	
$\mu_{TR}$	-	
$t_{3.1}$	-	Bailey Coefficients
$t_{3.2}$	-	
$t_{3.3}$	-	
$t_{4.1}$	-	
$t_{4.2}$	-	
$t_{4.3}$	-	
$t_{4.4}$	-	
$t_{4.5}$	-	
$t_{4.6}$	-	
$t_{5.1}$	-	
$t_{5.2}$	-	
$t_{5.3}$	-	
$t_{5.4}$	-	
$t_{5.5}$	-	
$t_{5.6}$	-	
$t_{5.7}$	-	
$t_{5.8}$	-	
$t_{5.9}$	-	
$t_{5.10}$	-	
B	-	
G	1/RADS	Blade section lift curve slope (2D)
$A_{TR}$	-	Actual number of blade on the tail rotor
$b_{TR}$	FT	Blade Chord for the Tail rotor
$C_{TR}$	DEG	Tail rotor commanded blade pitch

**Table A.4 (Continue):** Notations for the tail rotor module.

$C_{QTR}$	-	Tail rotor torque coefficient
$T_{TR}$	LB	Tail Rotor Thrust
$\frac{\partial a_0}{\partial T_{TR}}$	-	Rate of change of coning with thrust
$\delta_3$	DEG	Flapping hinge offset angle
$B_{IASTR}$	DEG	Blade pitch correction to linear twist
$\theta_{TR}$	DEG	Actual blade pitch
$D_{WSHTR}$	-	Uniform downwash at the tail rotor disc
$T_{WSTTR}$	DEG/R_TR	Linear blade twist
$\lambda_{TR}$	-	Tail rotor inflow
$K_{BLKTR}$	-	Tail rotor blockage from vertical tail
$C_{DTR}$	FT <sup>2</sup>	Tail rotor drag
$\rho$	SLUGS/FT <sup>3</sup>	Air density
$X_{TR}$	LB	Tail rotor forces at the CG in body axes
$Y_{TR}$	LB	
$Z_{TR}$	LB	
$L_{TR}$	FT LB	Tail rotor moments at the CG in body axes
$M_{TR}$	FT LB	
$N_{TR}$	FT LB	



## **RESUME**

### **PERSONNEL INFORMATION**

Name Surname : Osman AYCI  
Date of Birth : 23.01.1987  
E-mail : osmanayci@gmail.com  
Phone : +90 533 139 7515

### **EDUCATION**

High School : Nermin Mehmet Çekiç Anatolian High School - 2006  
Bachelor of Science : Middle East Technical University,  
Faculty of Engineering,  
Aerospace Engineering Department - 2012  
Master of Science : University of Turkish Aeronautical Association,  
Institute of Science and Technology,  
Mechanical and Aeronautical Engineering - Present

### **EXPERIENCE**

HAVELSAN, Modeling and Simulation Engineer 2013 – Present

### **LANGUAGE**

English